52p.

NASA TECHNICAL MEMORANDUM

NASA TM X-831

X63 16194

Code 2

NASA TM X-831

STATIC LONGITUDINAL AND LATERAL STABILITY AND CONTROL CHARACTERISTICS OF A RIGHT TRIANGULAR PYRAMIDAL LIFTING REENTRY CONFIGURATION AT MACH NUMBERS FROM 2.36 TO 4.65 (U)

[6]

by Nickolai Charczenko and G. Donald Babb

National Aeronautics and Space Administration
Langley Research Center,
Langley Station, ~~Hampton~~, Va.

Washington, NASA, Sept. 1963
52p. Tmp

NATIONAL AERONAUTICS AND SPACE ADMINISTRATION • WASHINGTON, D. C. • SEPTEMBER 1963

[redacted]

TECHNICAL MEMORANDUM X-831

STATIC LONGITUDINAL AND LATERAL STABILITY AND CONTROL CHARACTERISTICS OF A RIGHT TRIANGULAR PYRAMIDAL LIFTING REENTRY CONFIGURATION AT MACH NUMBERS FROM 2.36 TO 4.65

By Nickolai Charczenko and C. Donald Babb

Langley Research Center
Langley Station, Hampton, Va.

NATIONAL AERONAUTICS AND SPACE ADMINISTRATION

NATIONAL AERONAUTICS AND SPACE ADMINISTRATION

TECHNICAL MEMORANDUM X-831

STATIC LONGITUDINAL AND LATERAL STABILITY AND CONTROL CHARACTERISTICS OF A RIGHT TRIANGULAR PYRAMIDAL LIFTING REENTRY CONFIGURATION AT MACH NUMBERS FROM 2.36 TO 4.65*

By Nickolai Charczenko and C. Donald Babb

SUMMARY

An investigation has been conducted to determine the static longitudinal and lateral stability and control characteristics of a right triangular pyramidal lifting reentry configuration at Mach numbers from 2.36 to 4.65. The configuration had a 45° dihedral angle on the lower surfaces, a sweepback angle of 79.5°, and was triangular both in planform and cross section. Modifications to the basic configuration included a boattail extension to the body and the addition of speed brakes. Tests were conducted over an angle-of-attack range from about 2° to 30° and an angle-of-sideslip range from about -5° to 10°. The Reynolds number for the tests varied from 0.88×10^6 to 2.07×10^6, depending on Mach number.

The results of this investigation indicated that the three hypersonic glider models are longitudinally, laterally, and directionally stable about the center-of-gravity location chosen. A lift-drag ratio of about 2.9 may be obtained for the boattail configuration at a Mach number of 4.65. It appears that for the center-of-gravity location chosen for these tests, the basic configuration is trimmable with the top-mounted flap controls up to lift coefficients near maximum lift-drag ratio at Mach numbers to 2.87; however, trim difficulties may be encountered at higher lift coefficients. Roll control may be obtained on the basic configuration with either the 10° top-mounted flap or the 10° side-mounted flap in its upper position; however, roll control rapidly loses effectiveness for the top-mounted flap with increase in angle of attack, and adverse yawing moments are encountered with the side-mounted flap arrangements. There is little or no roll control produced by 10° side-mounted flaps on the boattail configuration. The side-mounted flaps on this configuration, however, produce an adverse yaw effect for the model.

* Title, Unclassified.

INTRODUCTION

Among the current programs in space research is the development of a suitable vehicle configuration for use as a long-range, manned entry glider. Design of such a vehicle, of course, will be dependent upon its specific mission requirements. The National Aeronautics and Space Administration has been investigating several configurations of such a glider having a pyramidal shape with a 45° dihedral and a leading-edge sweep of 79.5°. The results of these investigations in the subsonic, transonic, and hypersonic speed ranges may be found in references 1 to 7.

The purpose of the present investigation was to determine the static aerodynamic and control characteristics of pyramidal configurations in the supersonic Mach number range. The investigation was conducted in the Langley Unitary Plan wind tunnel, at Mach numbers from 2.36 to 4.65, over an angle-of-attack range from about 2° to 30° and an angle-of-sideslip range from -5° to 10°.

SYMBOLS

The aerodynamic forces and moments are referred to the stability axis for the longitudinal data and to the body axis for the sideslip data. (See fig. 1). The moment center is located at a point 21.53 inches aft of the nose and 2.14 inches above the reference line for all three test configurations. (See fig. 2.)

A	base area used in base-drag computation (for speed brake and basic configurations, 0.289 sq ft; for boattail configuration, 0.129 sq ft)
$\bar{c}$	wing mean aerodynamic chord, ft
C_D	drag coefficient, D/qS
$C_{D,b}$	base-drag coefficient, $\frac{(p_\infty - p_b)A}{qS}$
$C_{D,min}$	minimum drag coefficient
C_L	lift coefficient, L/qS
C_l	rolling-moment coefficient, $\frac{\text{Rolling moment}}{qS\bar{c}}$
C_m	pitching-moment coefficient, $\frac{\text{Pitching moment}}{qS\bar{c}}$
C_n	yawing-moment coefficient, $\frac{\text{Yawing moment}}{qS\bar{c}}$
C_Y	side-force coefficient, $\frac{\text{Side force}}{qS}$

C_{L_α}	lift-curve slope, $\partial C_L/\partial\alpha$
$C_{m_{C_L}}$	pitching-moment-curve slope, $\partial C_m/\partial C_L$
D	drag, lb
L	lift, lb
L/D	lift-drag ratio, C_L/C_D
$(L/D)_{max}$	maximum lift-drag ratio
M	free-stream Mach number
p_b	base pressure, lb/sq ft
p_t	free-stream stagnation pressure, lb/sq ft
p_∞	free-stream static pressure, lb/sq ft
q	free-stream dynamic pressure, lb/sq ft
R	Reynolds number per foot
S	projected wing planform area of basic configuration, sq ft
T_t	stagnation temperature, °F
α	angle of attack referred to X-axis (body reference line), deg
β	angle of sideslip referred to body plane of symmetry, deg
ΔC_l	incremental rolling-moment coefficient $\left(C_{l,\beta=5^\circ} - C_{l,\beta=0^\circ}\right)$
$\Delta C_l'$	incremental rolling-moment coefficient due to flap deflection
ΔC_n	incremental yawing-moment coefficient $\left(C_{n,\beta=5^\circ} - C_{n,\beta=0^\circ}\right)$
$\Delta C_n'$	incremental yawing-moment coefficient due to flap deflection
ΔC_Y	incremental side-force coefficient $\left(C_{Y,\beta=5^\circ} - C_{Y,\beta=0^\circ}\right)$
$\Delta C_Y'$	incremental side-force coefficient due to flap deflection
$\Delta C_l/\Delta\beta$	effective-dihedral parameter

$\Delta C_n/\Delta\beta$ directional-stability parameter

$\Delta C_Y/\Delta\beta$ side-force parameter

APPARATUS

Models

A model drawing with dimensional details is presented as figure 2 and photographs of the model are shown in figure 3.

The basic model is triangular both in cross section and in planform, and the nose of the model has been blunted. The lower surfaces of the model are considered as wings having 45° of dihedral and a projected sweepback angle of 79.5°. The boattail configuration consisted of the basic model with a 10-percent extension in length, the extension having a boattail angle of 20°. (See figs. 3 and 4.)

Aerodynamic control surfaces were employed on both the basic and the boattail models. (See fig. 4.) These controls consisted of 10° wedges with chords of 10 percent of the basic body length located on the aft portion of the model. The hinge line of the control was at the zero chord length of the control or wedge. When wedges were mounted on all three sides of the basic configuration, the resulting configuration was referred to as the speed-brake configuration.

Tunnel

Tests were conducted in both test sections of the Langley Unitary Plan wind tunnel. This tunnel is a variable-pressure, continuous, return-flow type with test sections 4 feet square and approximately 7 feet in length. An asymmetric sliding-block nozzle provides a means to vary the Mach number continuously from about 1.5 to 2.9 in the low Mach number test section and from about 2.3 to 4.7 in the high Mach number test section.

TESTS

Forces and moments acting on the model were measured with a six-component internal strain-gage balance. The model support system consisted of a sting-balance combination in connection with a remotely operated adjustable angle coupling which was attached to a tunnel central support system. Angle-of-attack variations were obtained with the adjustable angle coupling, and angle-of-sideslip variations were made through the central support system of the tunnel.

The pressures at the base of the model and in the balance chamber were measured by means of pressure transducers.

Tests were conducted over an angle-of-attack range from about 2° to 30° at an angle of sideslip of approximately 0° to determine the longitudinal aerodynamic and control characteristics of all configurations. The lateral stability and control characteristics were obtained over an angle-of-sideslip range from about -5° to 10° at an angle of attack of approximately 2°. Tunnel test conditions for the investigation are presented in the following table:

M	p_t, lb/sq in.	R	T_t, °F
2.36 2.87 2.98 3.71	6.3 6.3 10.6 20.2	1.16×10^6 .88 1.41 1.81	150
4.65	36.9	2.07×10^6	175

The dewpoint, measured at stagnation pressure, was maintained below -30° F in order to assure negligible condensation effects. Typical schlieren photographs of the model are shown in figure 5.

CORRECTIONS AND ACCURACY

All angles of attack and sideslip have been corrected for tunnel flow angularity and structural deflection of the sting-balance combination under aerodynamic load. The drag coefficients presented have not been adjusted for pressures acting on the base of the model; however, base pressure measurements were made, and the base-drag coefficients are presented in figure 6.

The maximum deviation of the local Mach number in the region of the tunnel occupied by the model is ±0.015 at Mach numbers to 3.71 and ±0.050 at a Mach number of 4.65. Estimated accuracies of the angles of attack and sideslip are within ±0.10°. The accuracies of the coefficients, based on calibration and repeatability of the data, are within the following limits:

C_L	±0.0010
C_m	±0.0020
C_D	±0.0020
C_l	±0.0005
C_n	±0.0015
C_y	±0.0040

PRESENTATION OF RESULTS

The results of the investigation are presented in the following figures:

RESULTS AND DISCUSSION

Longitudinal Characteristics

The basic aerodynamic characteristics in pitch for the three test configurations are presented in figure 7 and summarized in figure 8. The variation of lift coefficient with the angle of attack is practically linear for the entire angle-of-attack range; thus, in general, the analysis made at $C_L = 0$ will be applicable throughout the angle-of-attack range. The value of C_{L_α} of the basic configuration decreases from 0.0155 at $M = 2.36$ to a value of 0.013 at $M = 4.65$. The boattail configuration has slightly higher C_{L_α} values than those for the basic model throughout the test Mach number range; however, it should be pointed out that if the models were the same length, the C_{L_α} values for the basic configuration would be higher. As would be expected, the speed-brake configuration has the highest C_{L_α} values of any of the test vehicles and, for this configuration, there appears to be little or no change in C_{L_α} with Mach number (Reynolds number effect being neglected).

All the models are stable about the test center-of-gravity location and there are no large changes in stability with Mach number. The basic model is the least stable and the speed-brake model is the most stable. Here again the basic model would be more stable than the boattail model if it were of the same length.

Since the three models represent unpowered gliders, it should be emphasized in discussing drag coefficient and L/D comparisons that the drag coefficients have not been corrected for base pressure. Of the three configurations tested, the boattail model has the lower $C_{D,min}$ values and the higher $(L/D)_{max}$ values throughout the test Mach number range. The value of $(L/D)_{max}$ for this configuration at $M = 4.65$ is about 2.9. The highest $C_{D,min}$ value and the lowest $(L/D)_{max}$ value are obtained with the speed-brake configuration. These data show that the speed brakes are effective drag producers since the minimum drag

coefficients for the speed-brake configuration are about twice those for the other configurations at all test Mach numbers.

The effect of top-mounted flap controls on the pitch characteristics of the basic model at Mach numbers of 2.36 and 2.87 is presented in figure 9. The top-mounted half-span flap control leads to a loss in C_L and a slight decrease in C_{L_α}. The positive increment in C_m obtained with the half-span flap indicates that a full-span flap control on the top with a setting of 10° would probably trim the model near $(L/D)_{max}$ at both Mach numbers (M = 2.36 and 2.87); however, trim difficulties may be encountered at higher lift coefficients. From figure 9 it is apparent that the pitching-moment effectiveness of the control decreases at high angles of attack.

Lateral and Directional Characteristics

The basic aerodynamic characteristics in sideslip for the three test configurations are presented in figure 10. These data indicate that the test models are all laterally and directionally stable for all Mach numbers at which they were tested at an angle of attack of approximately 2°. There is little difference in the stability levels for the basic and the boattail configurations; however, as expected, the speed-brake configuration has a slightly greater positive dihedral effect and has more than double the directional stability of the other two configurations at the Mach numbers at which they were tested. The sideslip parameters $\Delta C_l/\Delta\beta$, $\Delta C_n/\Delta\beta$, and $\Delta C_Y/\Delta\beta$ are presented in figure 11 for angles of attack from about 2° to 30°. In general, the lateral and directional stability of the boattail configuration is greater than that for the basic body over this angle-of-attack range. The speed-brake configuration maintained a considerably greater stability level than the other two configurations in this angle-of-attack range. The stability of each configuration, furthermore, increases materially with increasing angle of attack.

The effect of various flaps on the lateral and directional control effectiveness of the basic and boattail models is presented in figure 12 for angles of attack from 4° to 28°. The top-mounted flap control is effective in producing roll at the lower angles of attack (near 4°); however, the effectiveness rapidly decreases with increase in angle of attack for both Mach numbers (2.36 and 2.87) at which this type of flap control was tested. This roll effectiveness is accompanied by a favorable yawing-moment increment at the lower angles of attack that gradually diminishes to zero at angles of attack above about 18°. With the flap mounted on the side of the basic model, only the arrangement with the flap in the upper position (which has the largest moment arm) produces any appreciable rolling moment. This moment increases with angle of attack and is little affected by Mach number. The yawing moment is adverse for all the side-mounted flap arrangements on the basic configuration, and this adverse effect increases with angle of attack. Only side-mounted flaps were tested with the boattail Configuration, and little roll effectiveness was obtained for this configuration throughout the angle-of-attack range at test Mach numbers. Appreciable adverse yawing moment, however, is encountered by all flap arrangements on the boattail configuration, and this adverse effect is significantly increased with increase in angle of attack.

CONCLUSIONS

An investigation conducted to determine the static longitudinal and lateral stability and control characteristics of a right triangular pyramidal lifting reentry configuration at Mach numbers from 2.36 to 4.65 indicates the following conclusions:

1. The three test models are longitudinally, laterally, and directionally stable about the center-of-gravity location chosen for these tests.

2. A lift-drag ratio of about 2.9 may be obtained for the boattail configuration at a Mach number of 4.65.

3. It appears that for the center-of-gravity location chosen for these tests, the basic configuration is trimmable with the top-mounted flap controls up to lift coefficients near maximum lift-drag ratio at Mach numbers to 2.87; however, trim difficulties may be encountered at higher lift coefficients.

4. Roll control may be obtained on the basic configuration with either the 10° top-mounted flap or the 10° side-mounted flap in its upper position; however, roll control rapidly loses effectiveness for the top-mounted flap with increase in angle of attack, and adverse yawing moments are encountered with the side-mounted flap arrangements.

5. There is little or no roll control produced by 10° side-mounted flaps on the boattail configuration. The side-mounted flaps on this configuration, however, produce an adverse yaw effect for the model.

Langley Research Center,
National Aeronautics and Space Administration,
Langley Station, Hampton, Va., April 26, 1963.

REFERENCES

1. Cooper, Morton, and Stainback, P. Calvin: Influence of Large Positive Dihedral on Heat Transfer to Leading Edges of Highly Swept Wings at Very High Mach Numbers. NASA MEMO 3-7-59L, 1959.

2. Paulson, John W.: Low-Speed Static Stability and Control Characteristics of a Model of a Right Triangular Pyramid Reentry Configuration. NASA MEMO 4-11-59L, 1959.

3. Olstad, Walter B., Mugler, John P., Jr., and Cahn, Maurice S.: Static Longitudinal and Lateral Stability Characteristics of a Right Triangular Pyramidal Lifting Reentry Configuration at Transonic Speeds. NASA TN D-655, 1961.

4. Whitcomb, Charles F., and Foss, Willard E., Jr.: Static Stability and Control Characteristics of Two Large-Dihedral Right Triangular Pyramid Lifting Reentry Configurations at a Mach Number of 3.05. NASA TM X-295, 1960.

5. Mayo, Edward E.: Static Longitudinal Stability Characteristics of a Blunted Glider Reentry Configuration Having 79.5° Sweepback and 45° Dihedral at a Mach Number of 6.2 and Angles of Attack up to 20°. NASA TM X-222, 1959.

6. Ware, George M.: Low-Subsonic-Speed Static Stability of Right-Triangular-Pyramid and Half-Cone Lifting Reentry Configurations. NASA TN D-646, 1961.

7. Cooper, Morton, and Gunn, Charles R.: Pressure Measurements on a Hypersonic Glide Configuration Having 79.5° Sweepback and 45° Dihedral at a Mach Number of 4.95. NASA TM X-223, 1959.

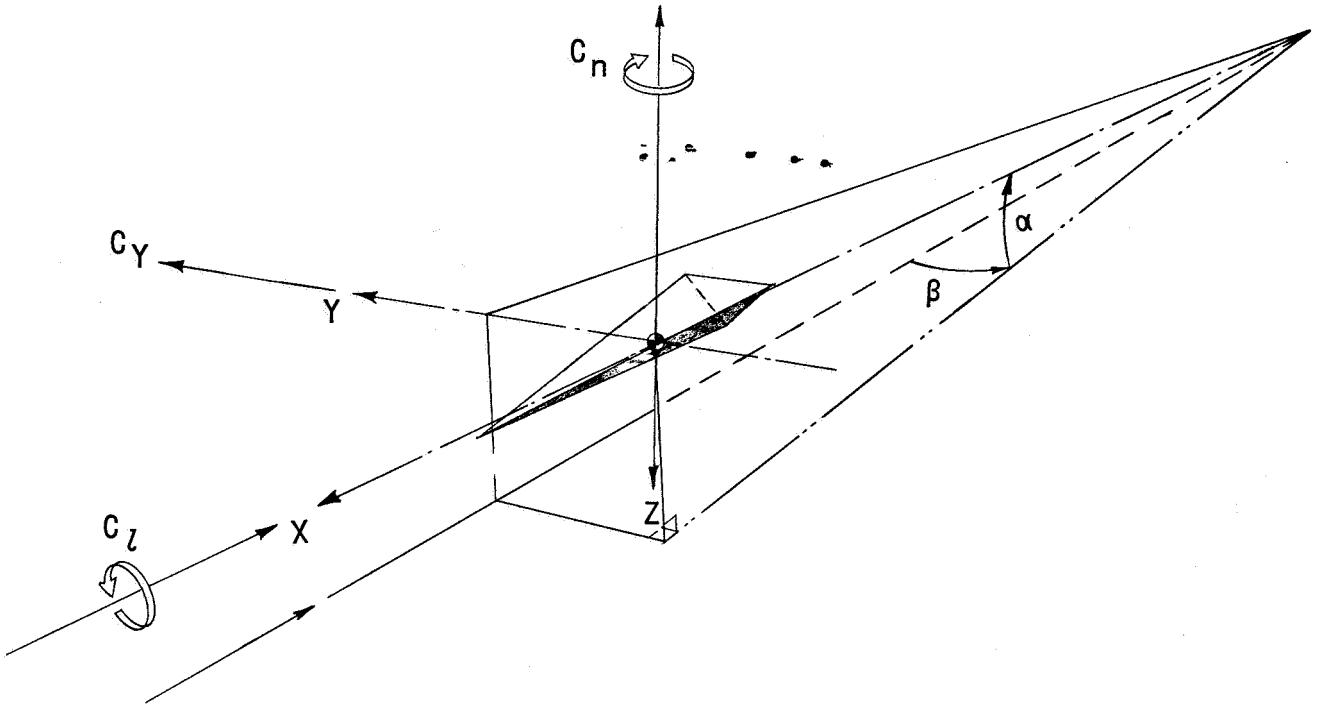

(a) Body axis.

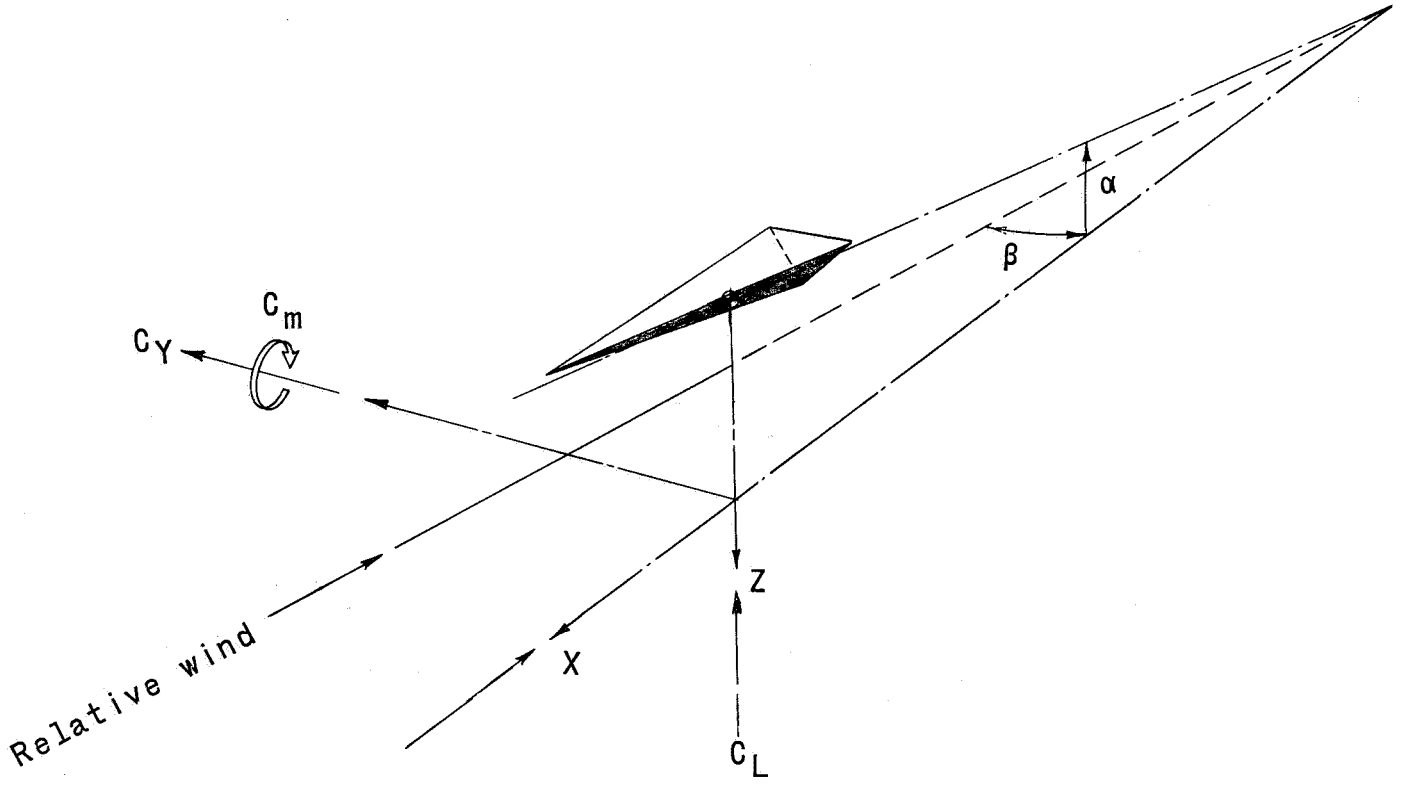

(b) Stability axis.

Figure 1.- System of axes. Arrows indicate positive directions.

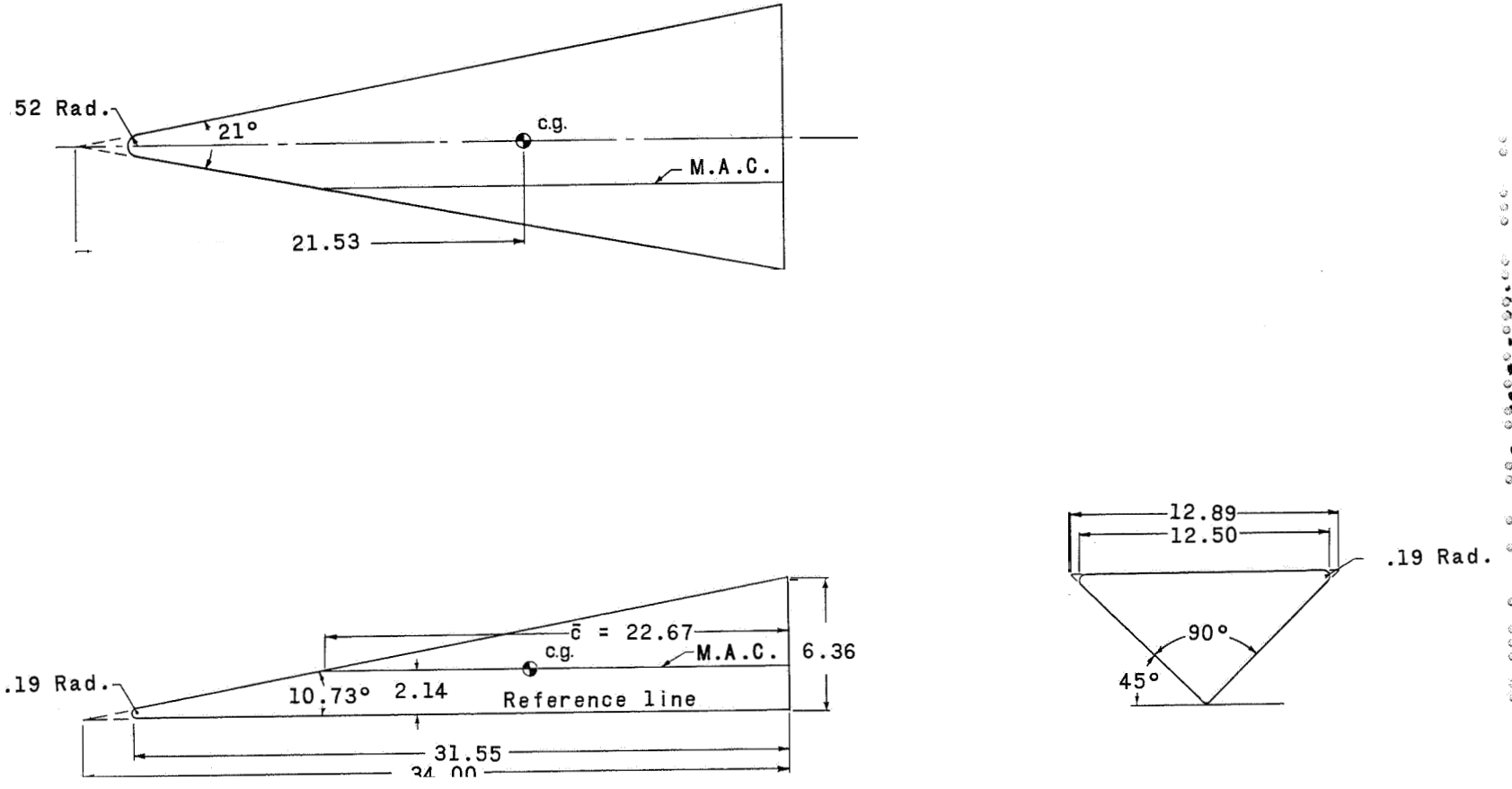

Figure 2.- Drawing of the basic configuration. (Dimensions are in inches unless otherwise specified.)

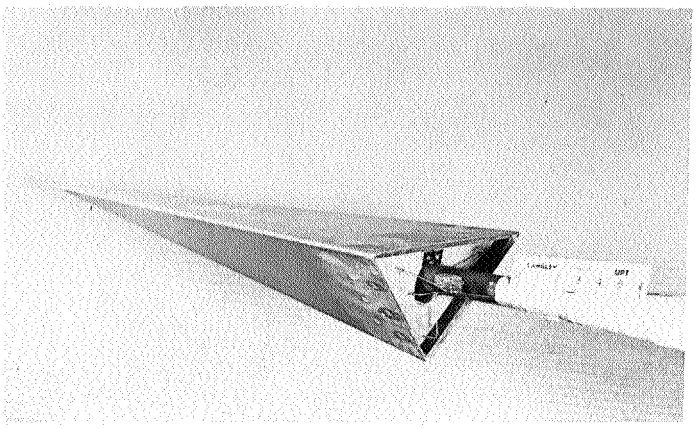

(a) Basic configuration.

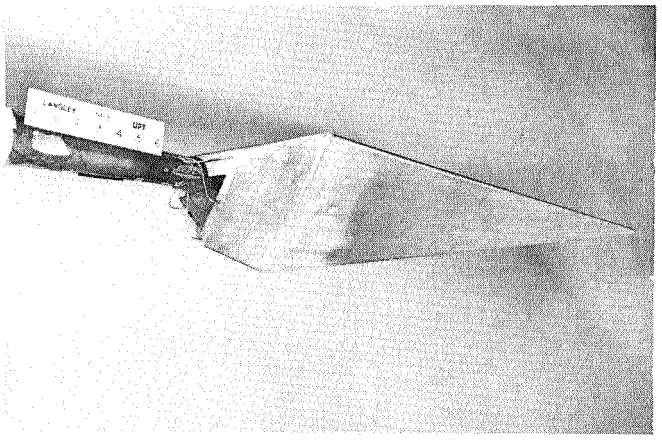

(b) Boattail configuration.

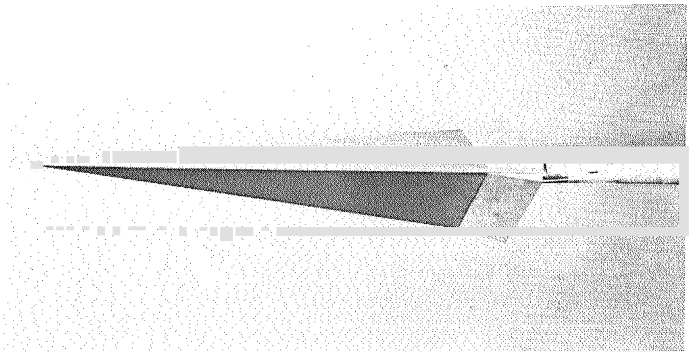

(c) Speed-brake configuration.

Figure 3.- Photographs of the three test configurations. L-63-3143

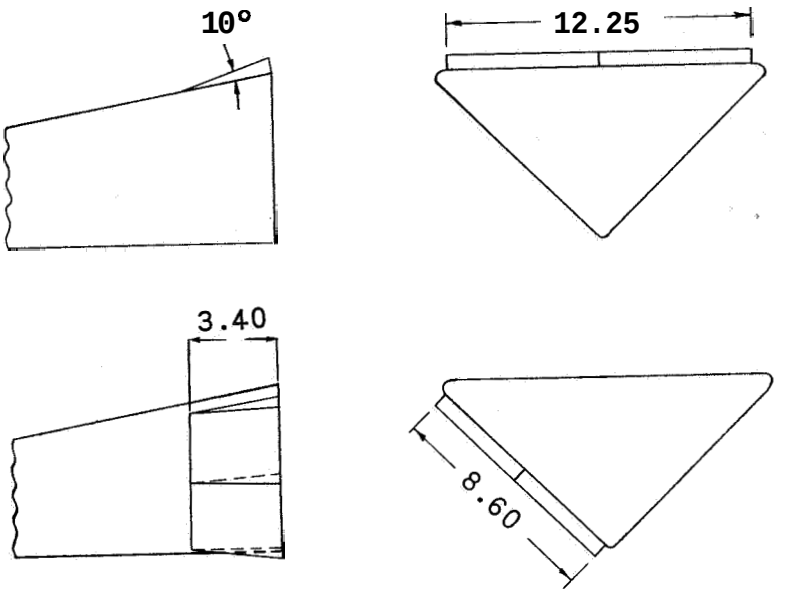

Basic configuration

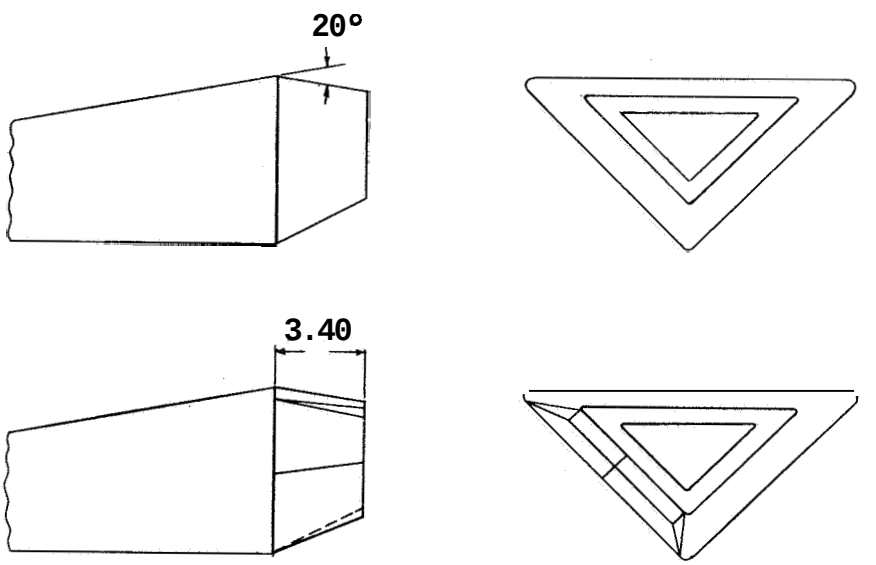

Boattail configuration

Figure 4.- Details of typical wedge-type control surfaces.

L-63-3144

(a) Basic configuration.

Figure 5.- Typical schlieren photographs.

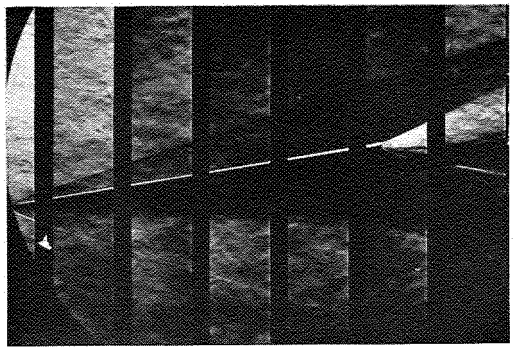

α = 2.0°

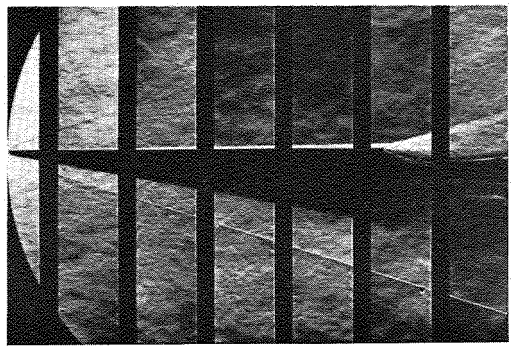

α = 11.1°

M = 3.71

α = 7.5°

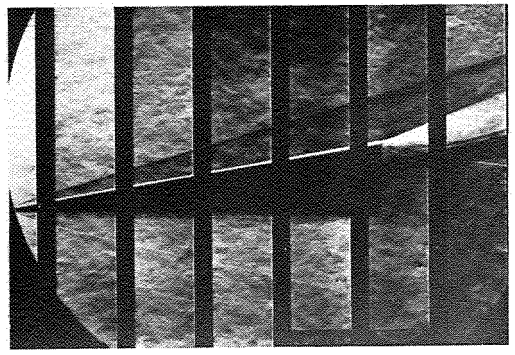

α = 2.7°

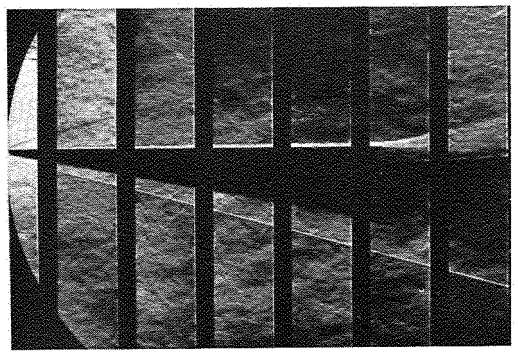

α = 11.8°

M = 4.65

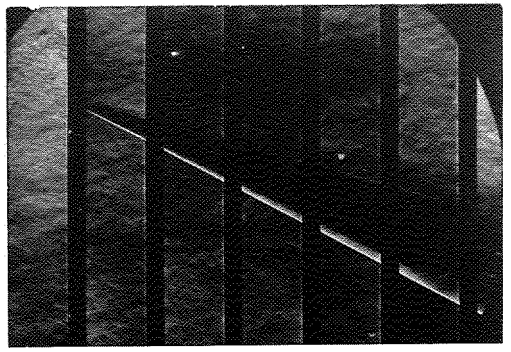

α = 28.0°

L-63-3145

(a) Concluded.

Figure 5.- Continued.

(b) Boattail configuration.

Figure 5.- Continued.

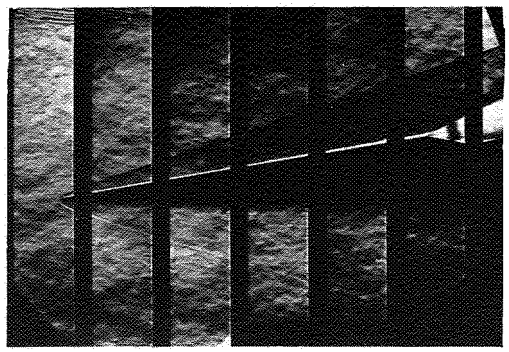

α = 1.9°

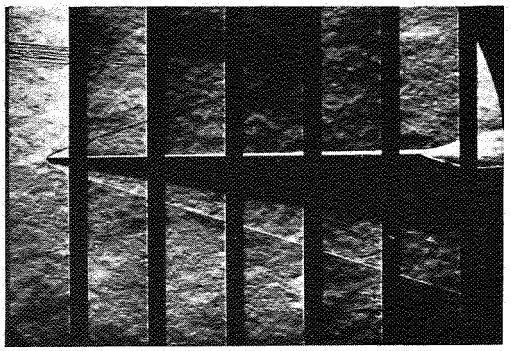

α = 11.0°

M = 3.71

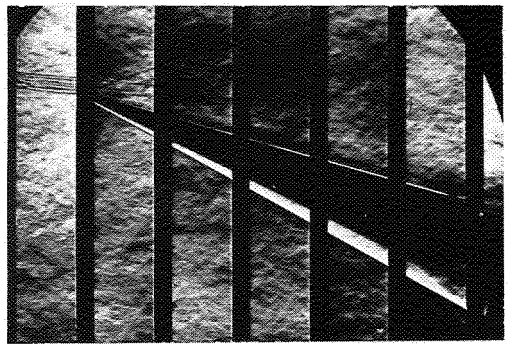

α = ≥ 3°

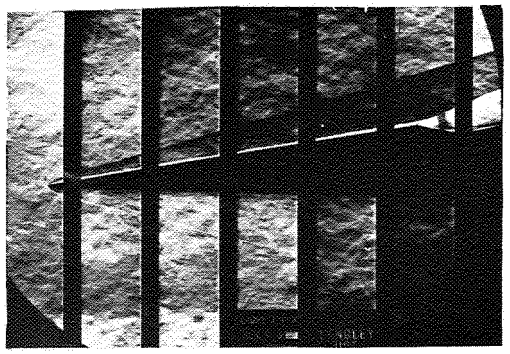

α = 7 ≤°

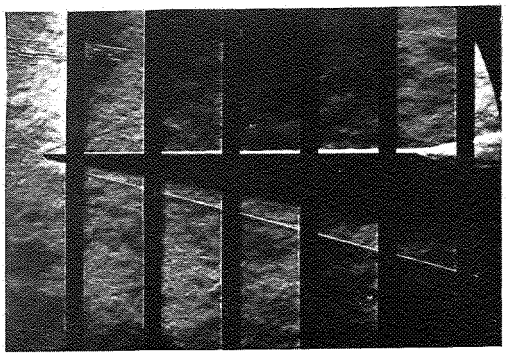

α = 11.7°

M = 4.65

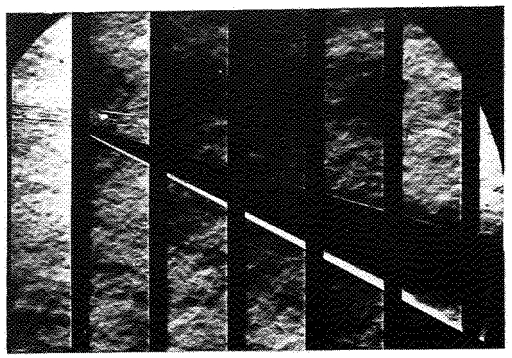

α = 7≤.0°

(b) Concluded.

L-63-3147

Figure 5 -

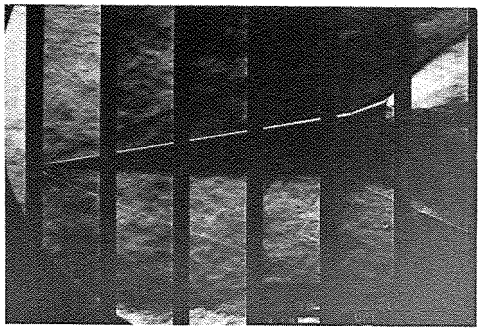

α = 1.9°

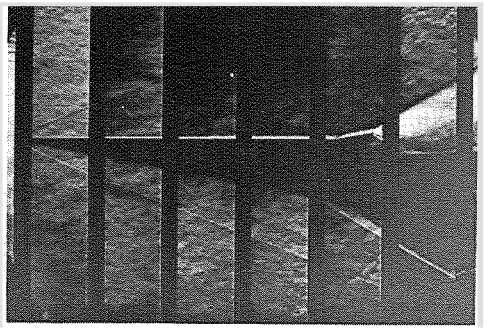

α = 11.0°
M = 2.98

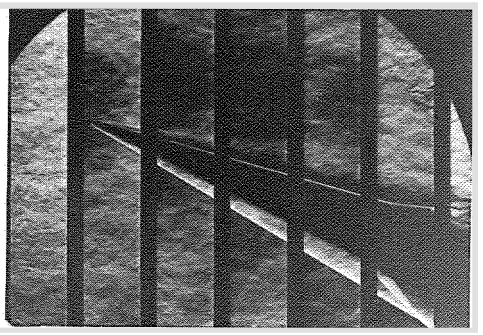

α = 27.3°

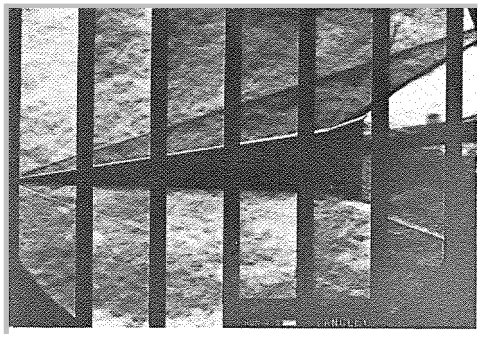

α = 2.0°

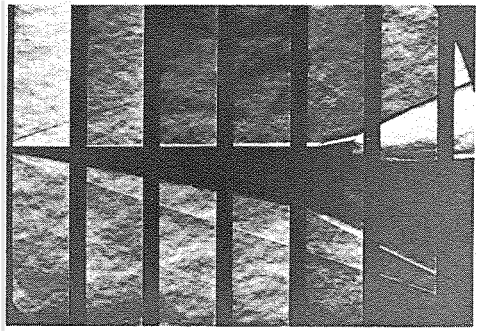

α = 11.1°
M = 3.71

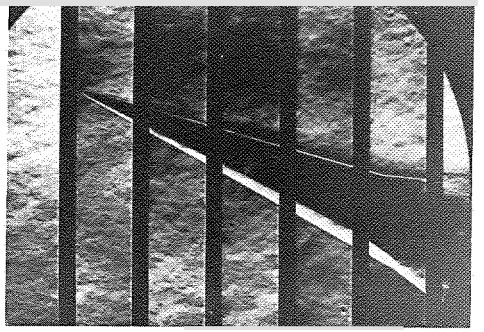

α = 27.3°

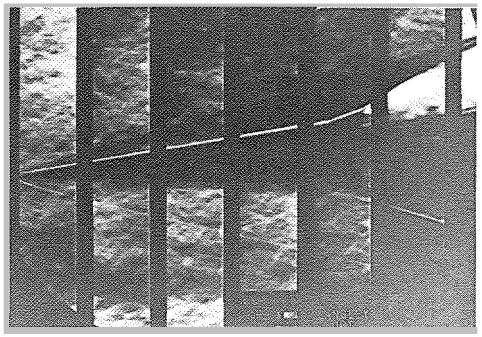

α = 2.7°

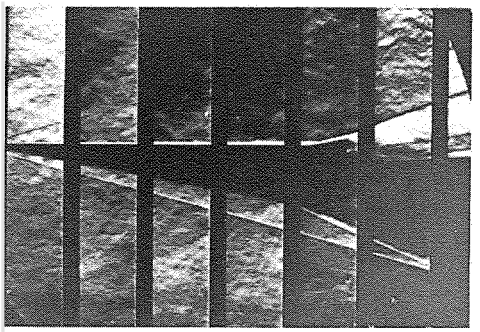

α = 11.7°
M = 4.65

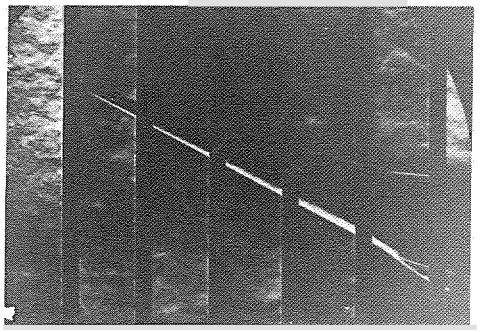

α = 27.9°

(c) Speed-brake configuration.

L-63-3148

Figure 5.- Concluded.

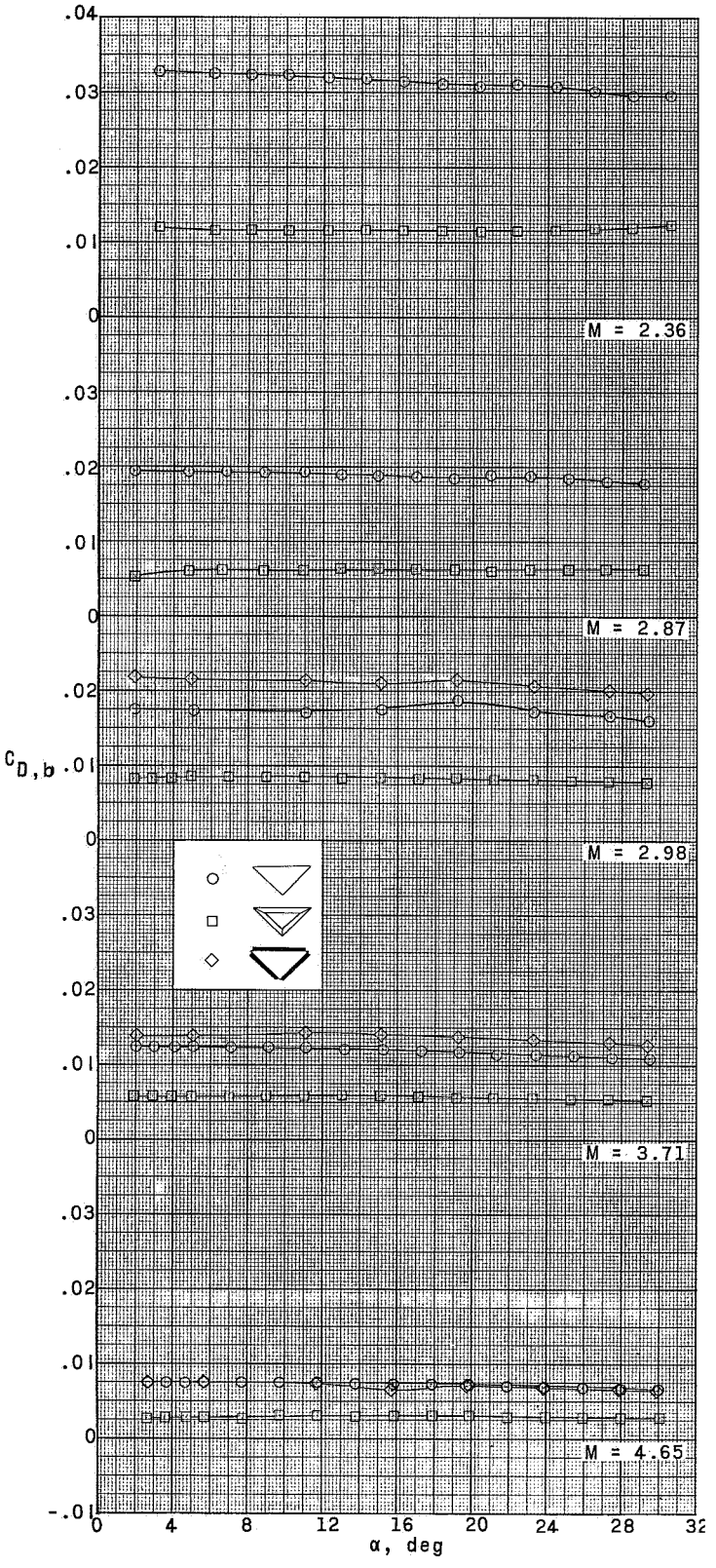

Figure 6.- Typical base-drag coefficients.

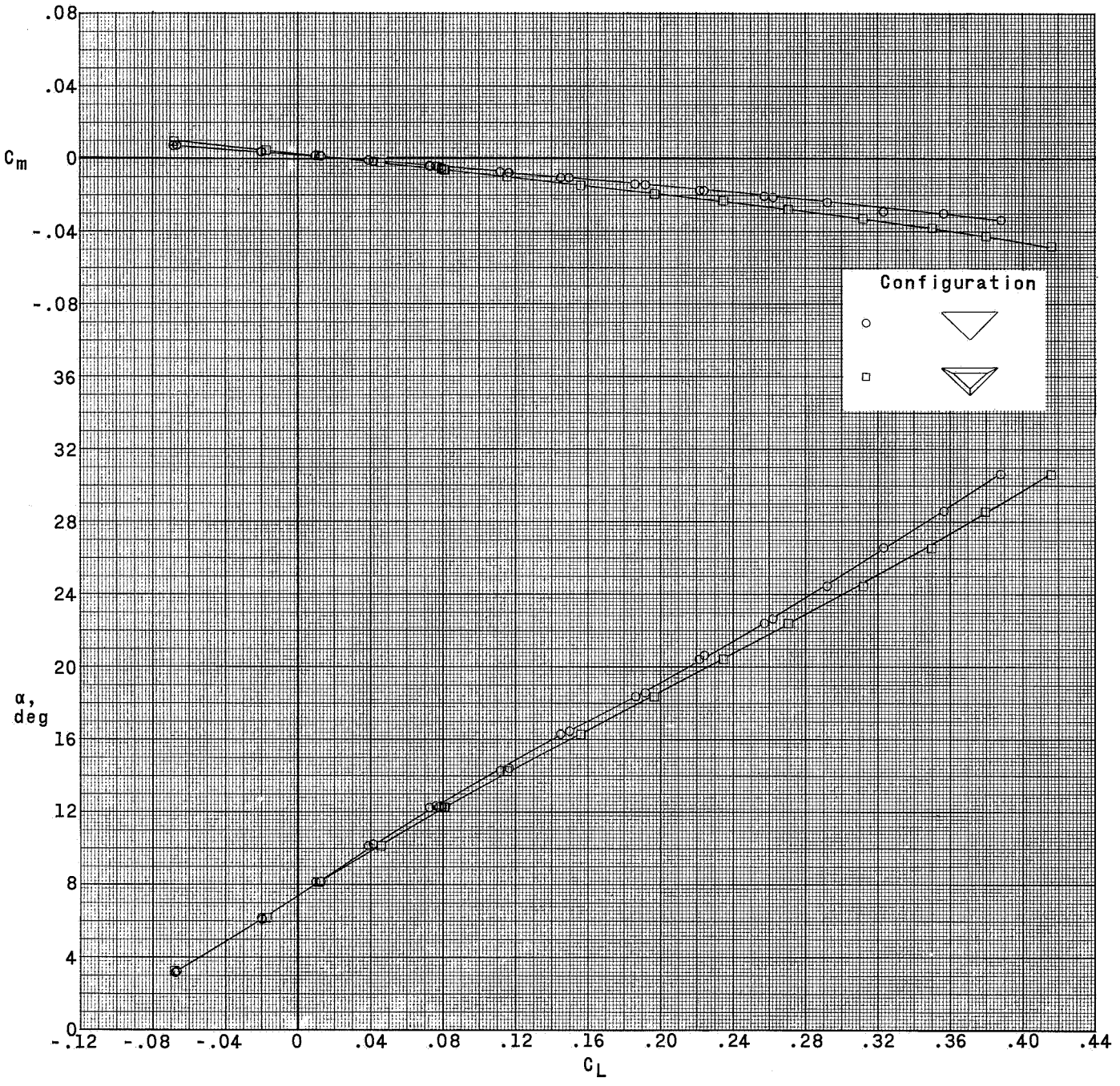

(a) M = 2.36.

Figure 7.- Aerodynamic characteristics in pitch for the three test configurations. $\beta \approx 0^{\circ}$.

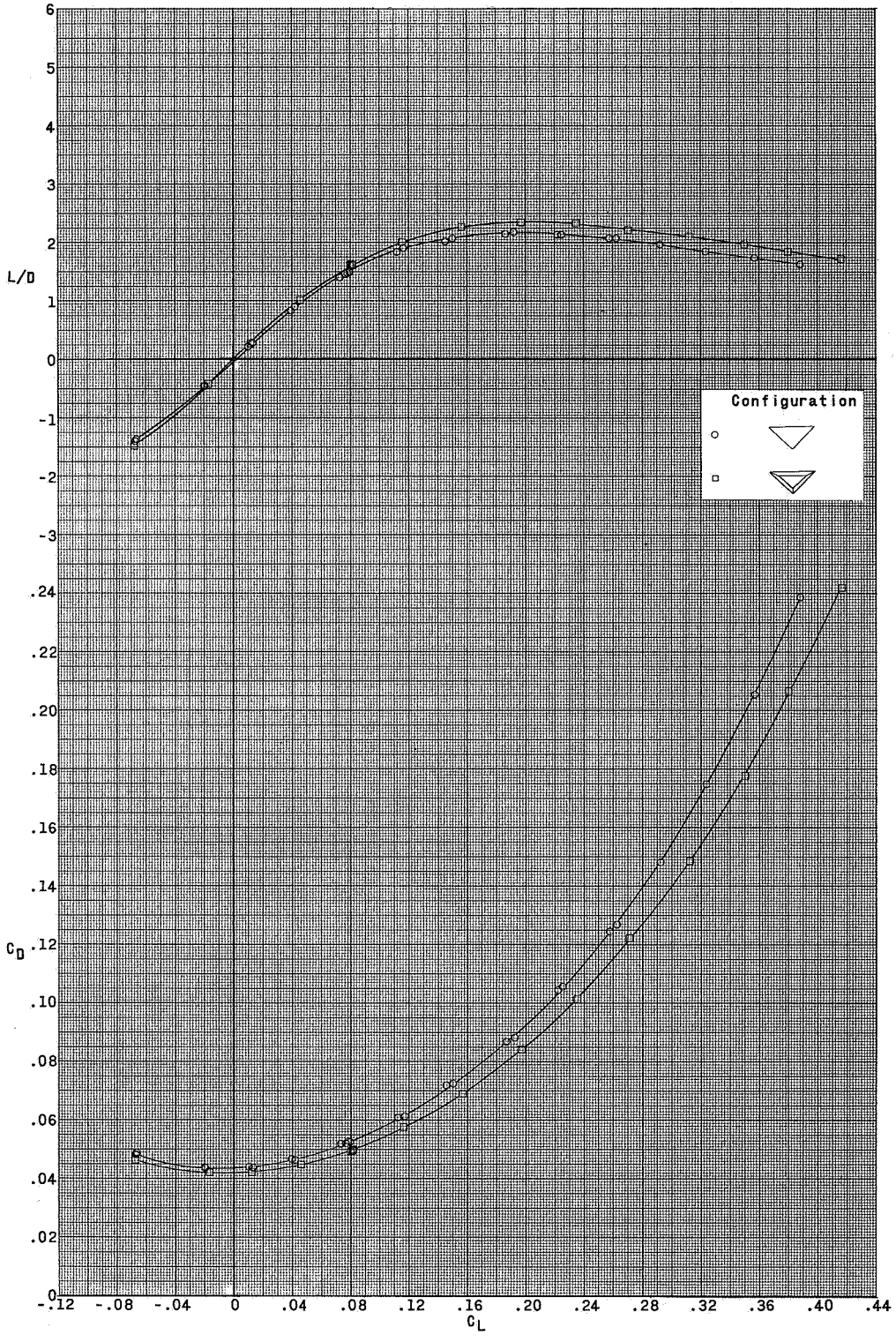

(a) Concluded.

Figure 7.- Continued.

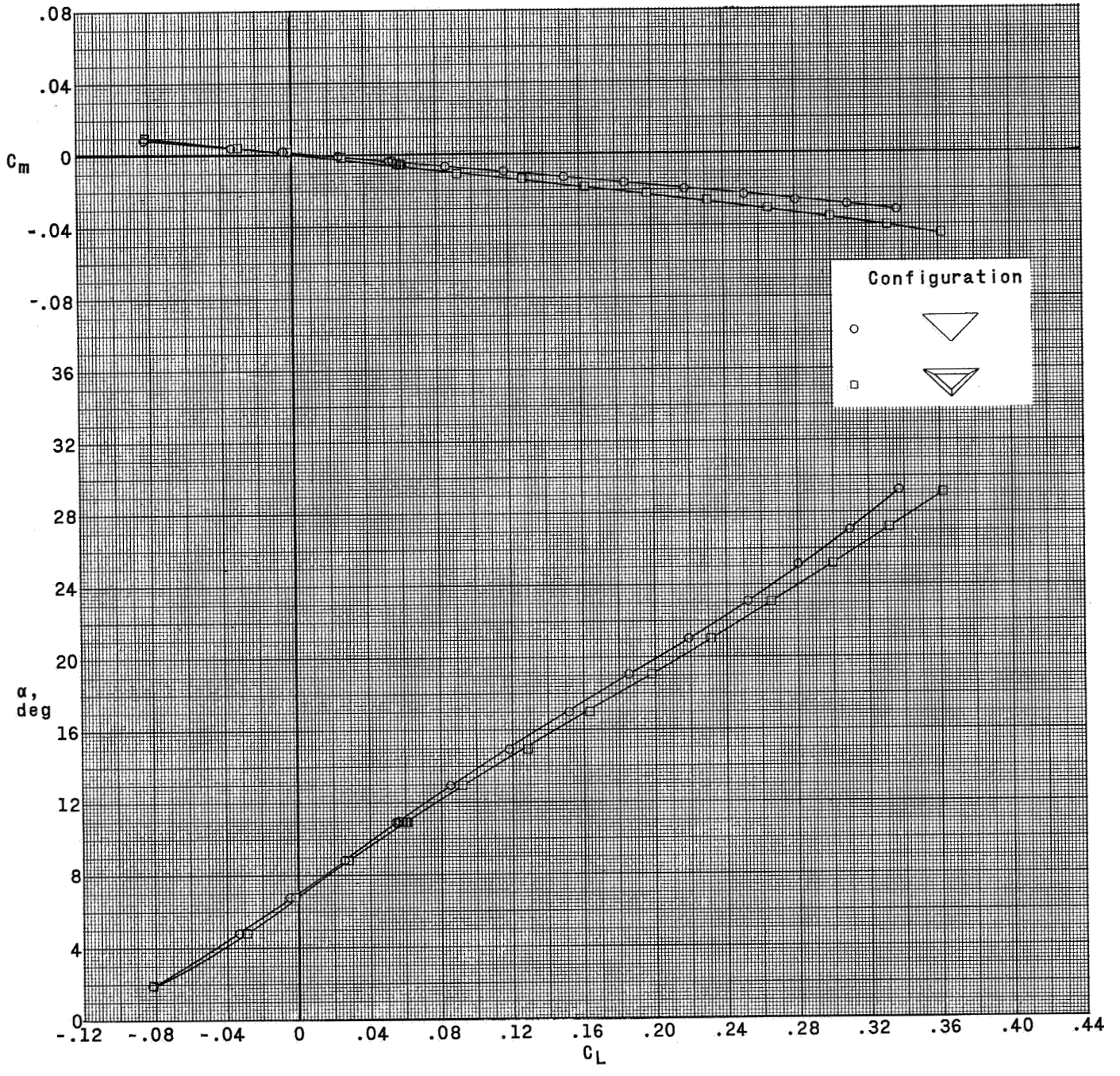

(b) M = 2.87.

Figure 7.- **Continued.**

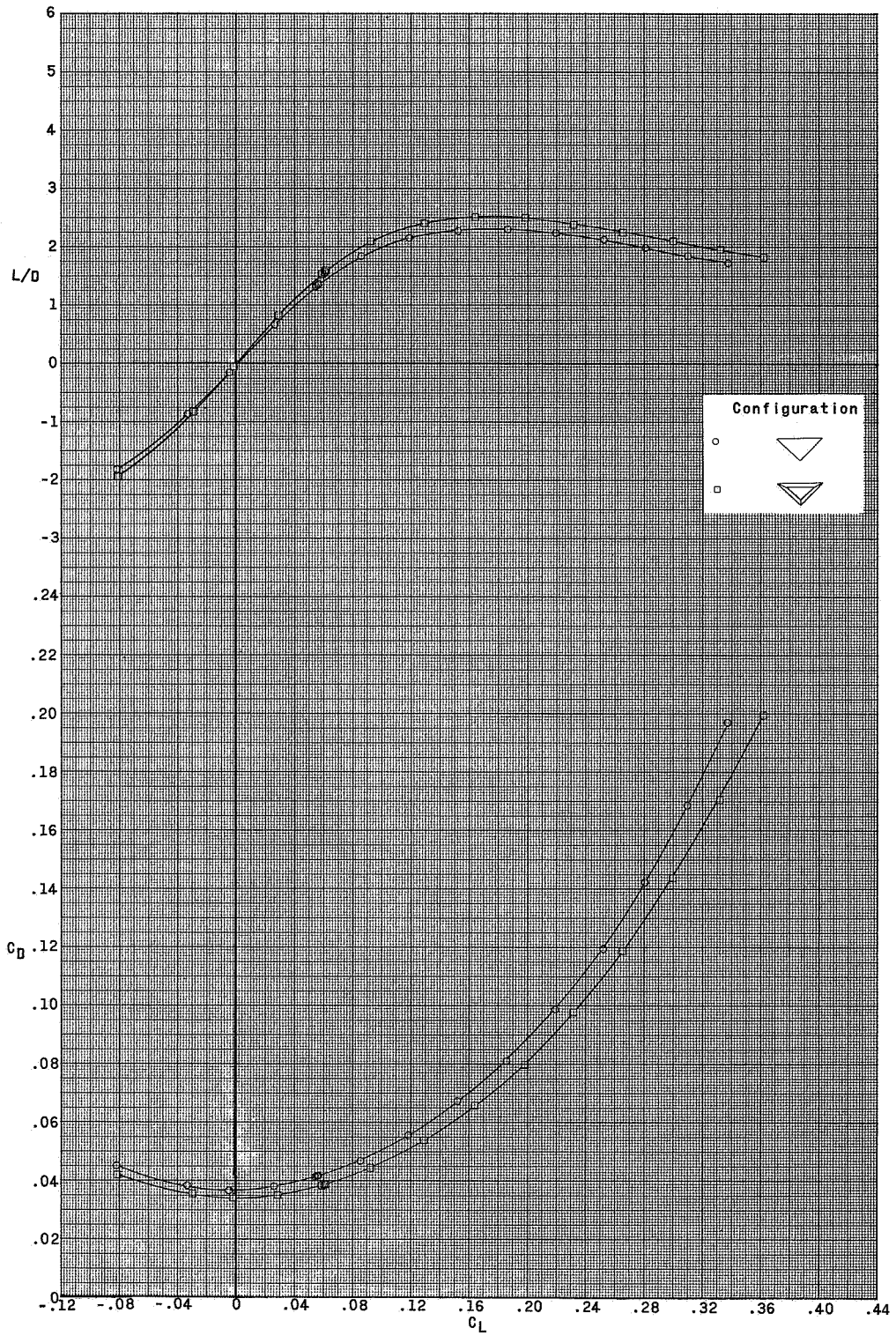

(b) Concluded.

Figure 7.- Continued,

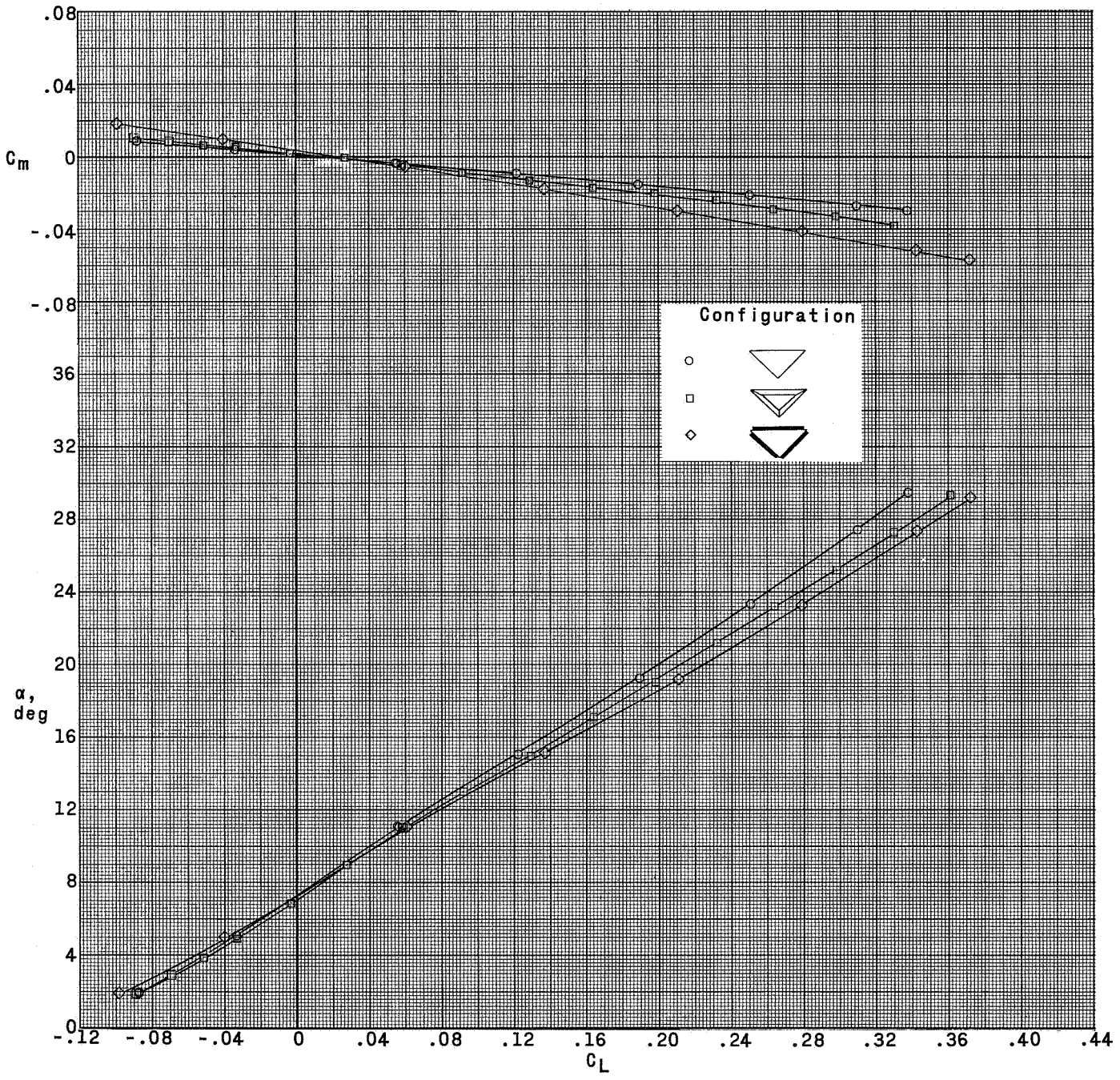

(c) M = 2.98.

Figure 7.- Continued.

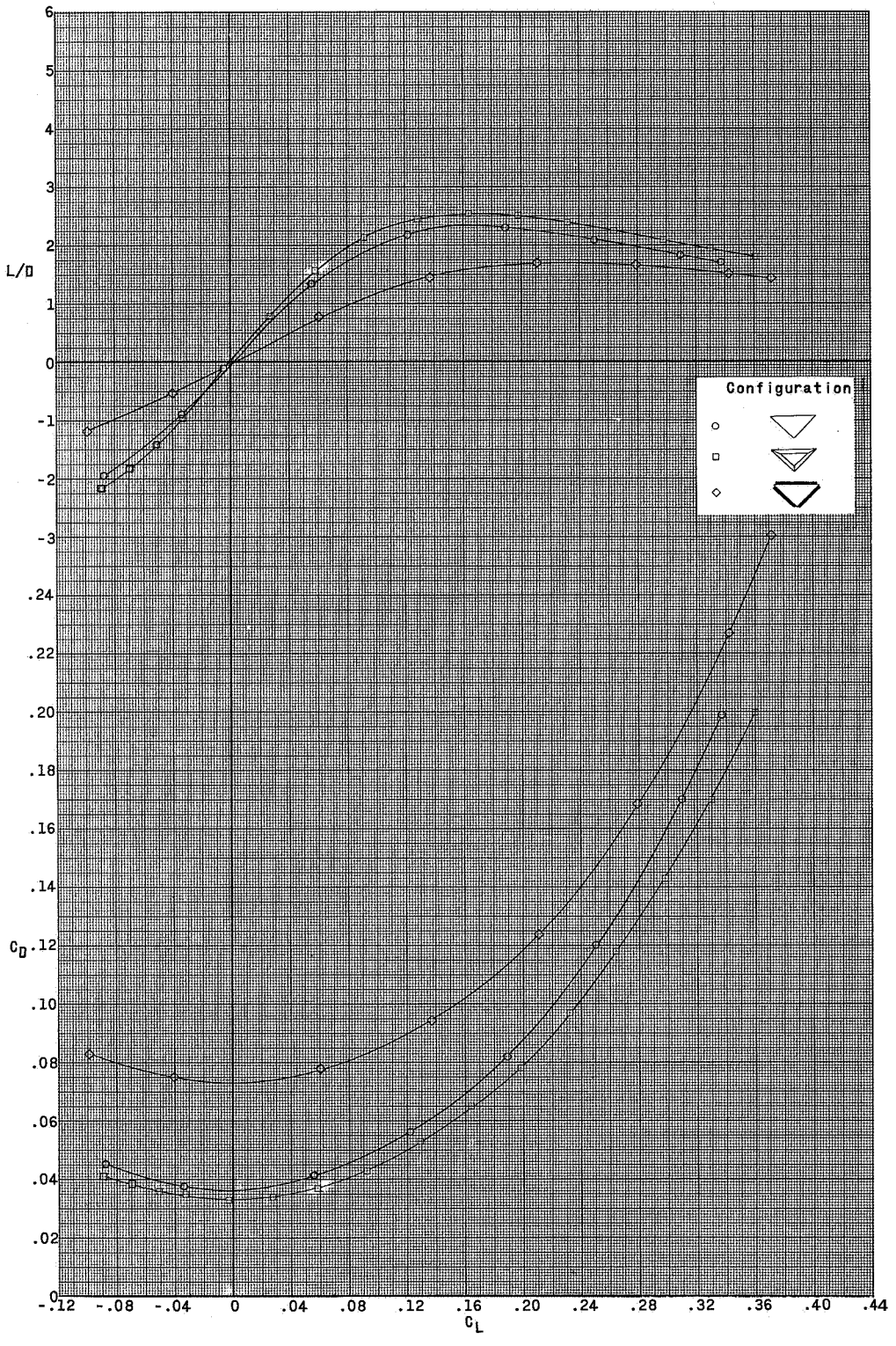

(c) Concluded.

Figure 7.- Continued.

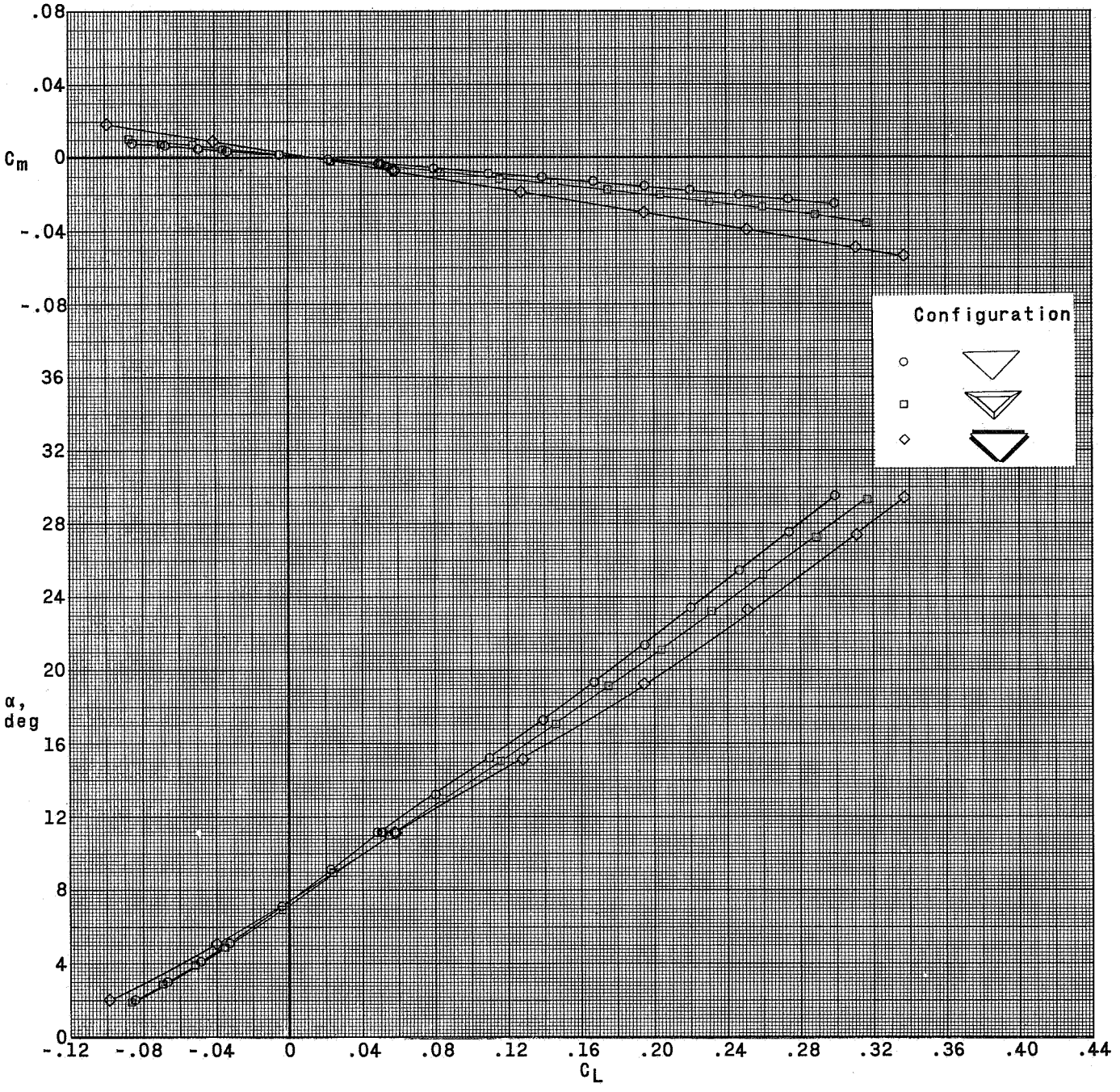

(d) M = 3.71.

Figure 7.- Continued.

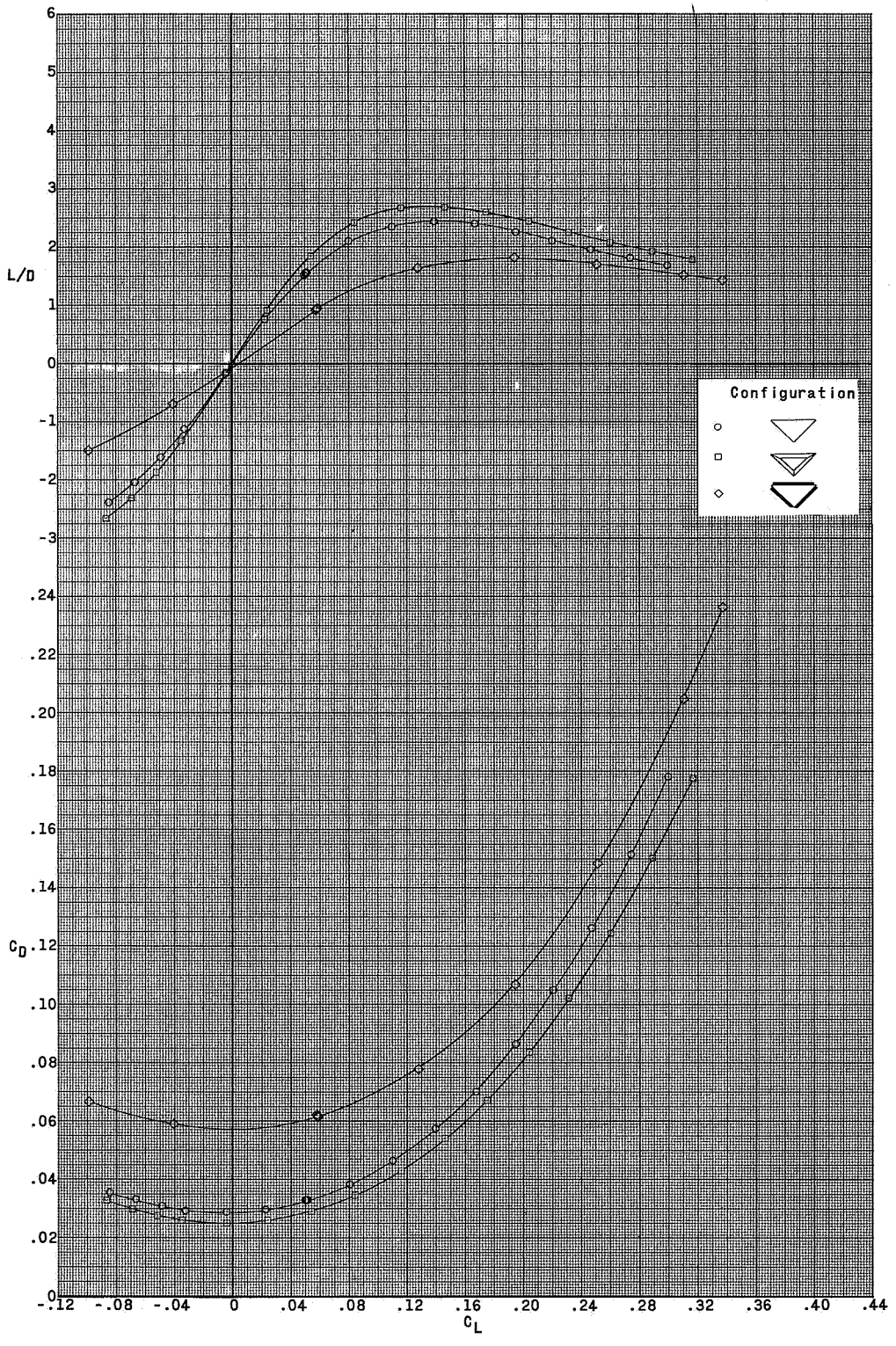

(d) Concluded.

Figure 7.- Continued.

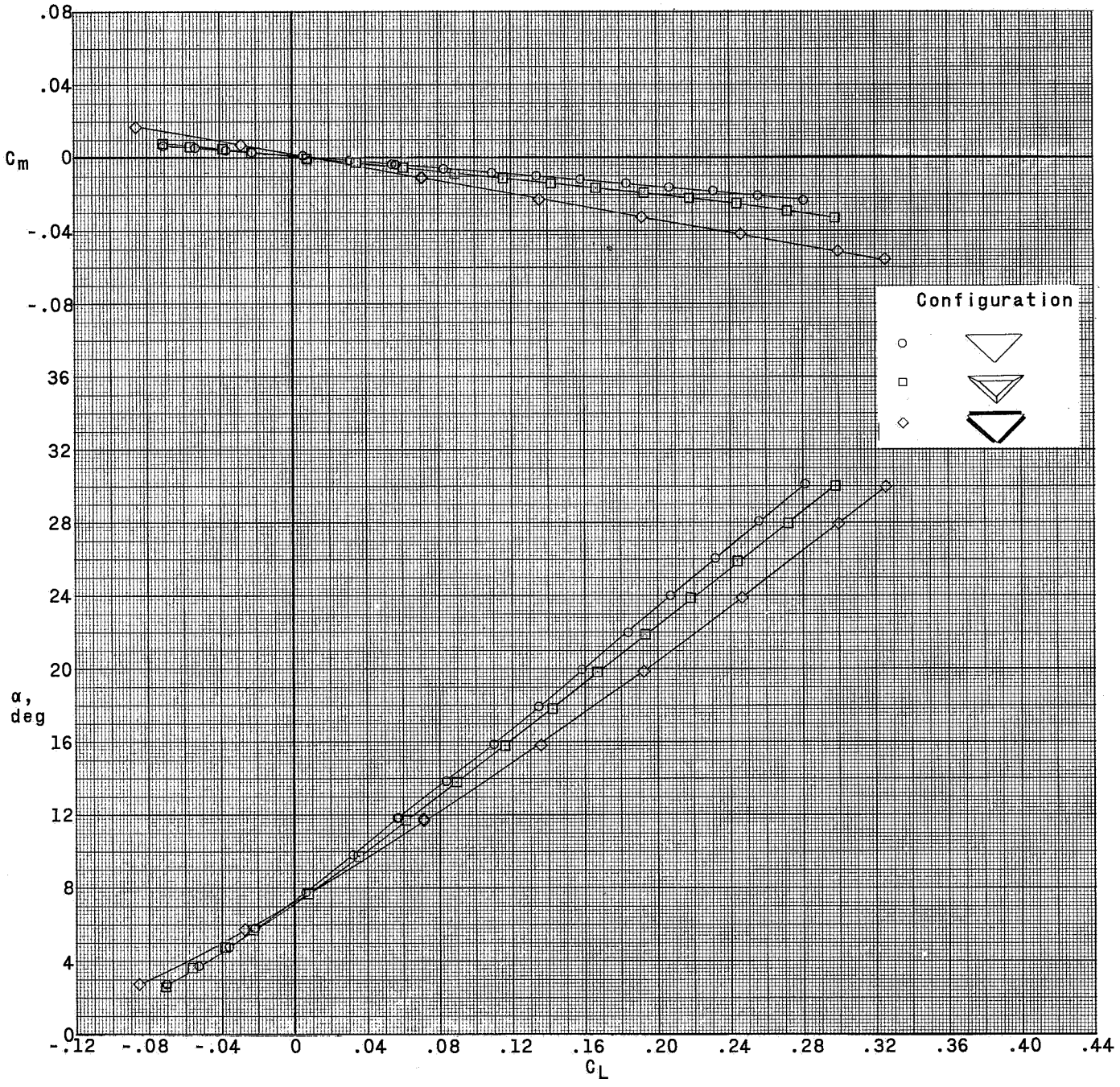

(e) M = 4.65.

Figure 7.- Continued.

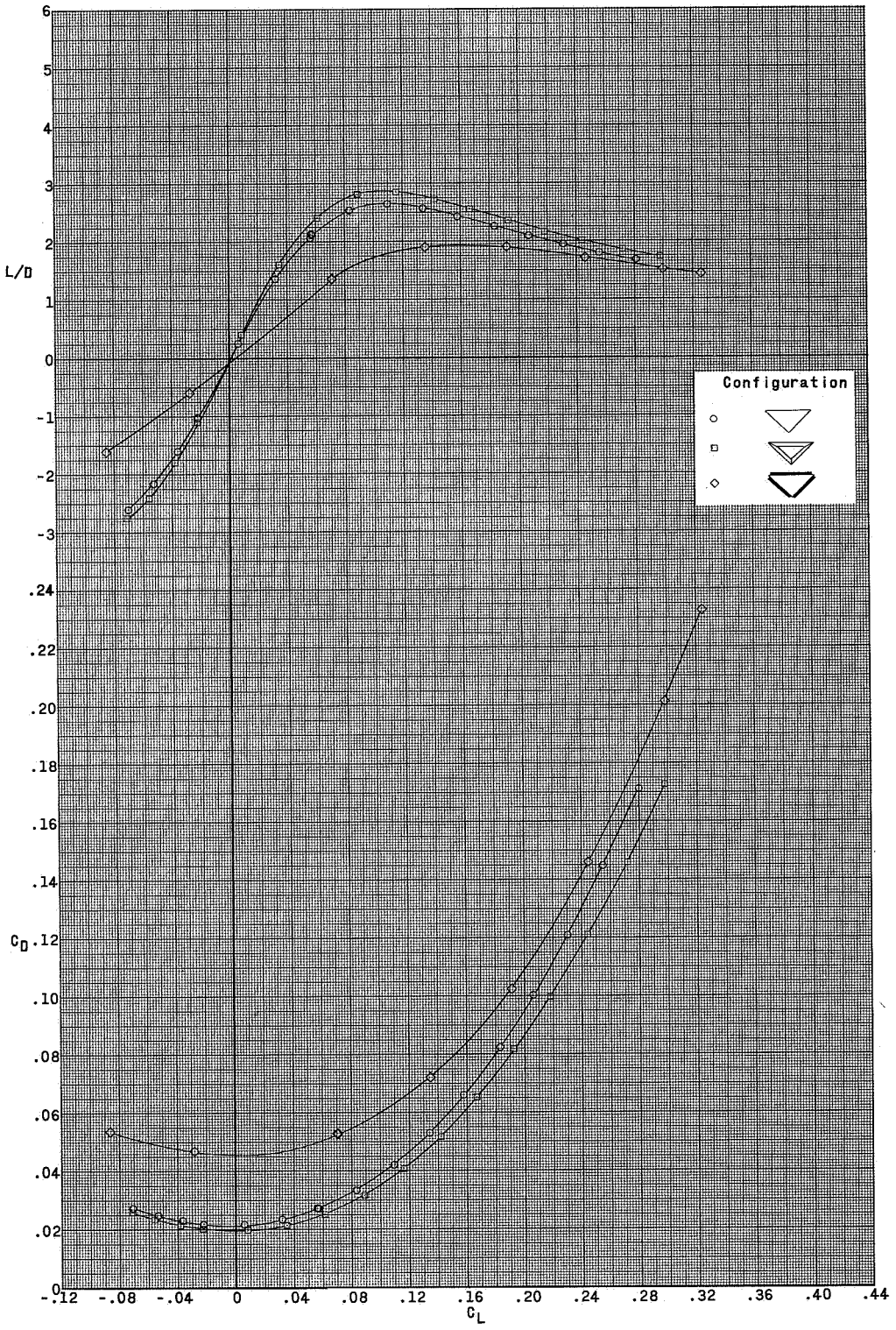

(e) Concluded.

Figure 7.- Concluded.

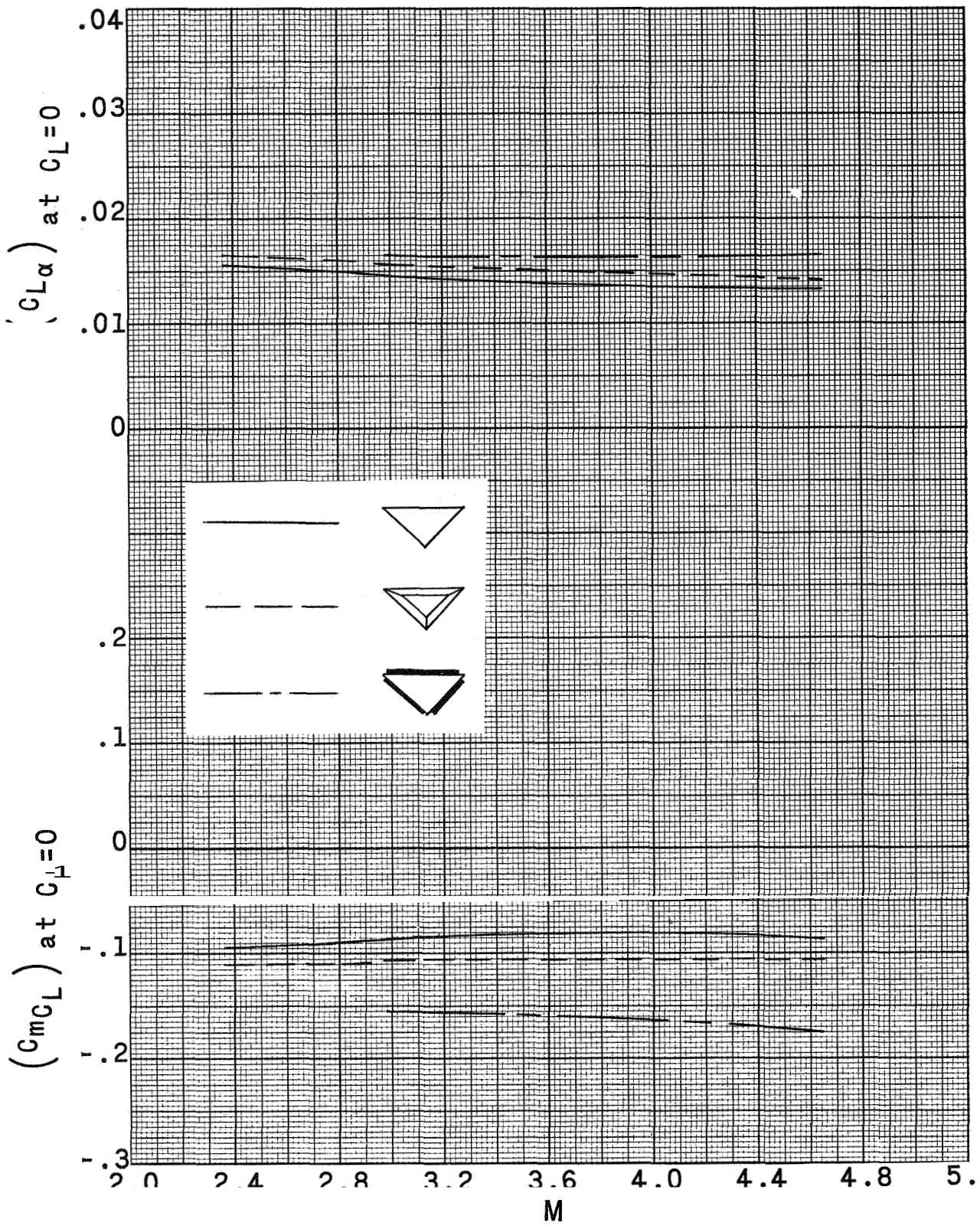

Figure 8.- Summary of aerodynamic characteristics in pitch.

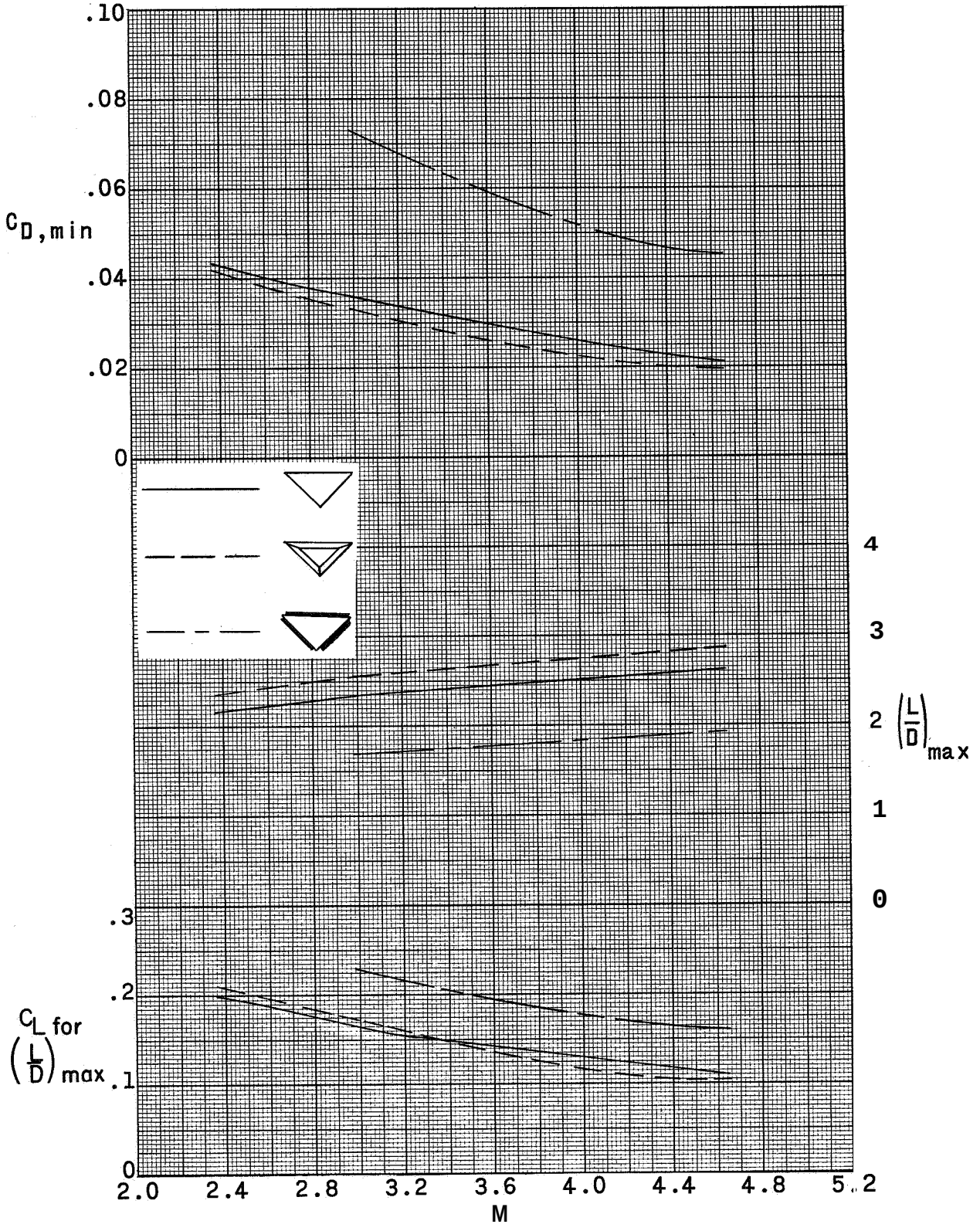

Figure 8.- Concluded.

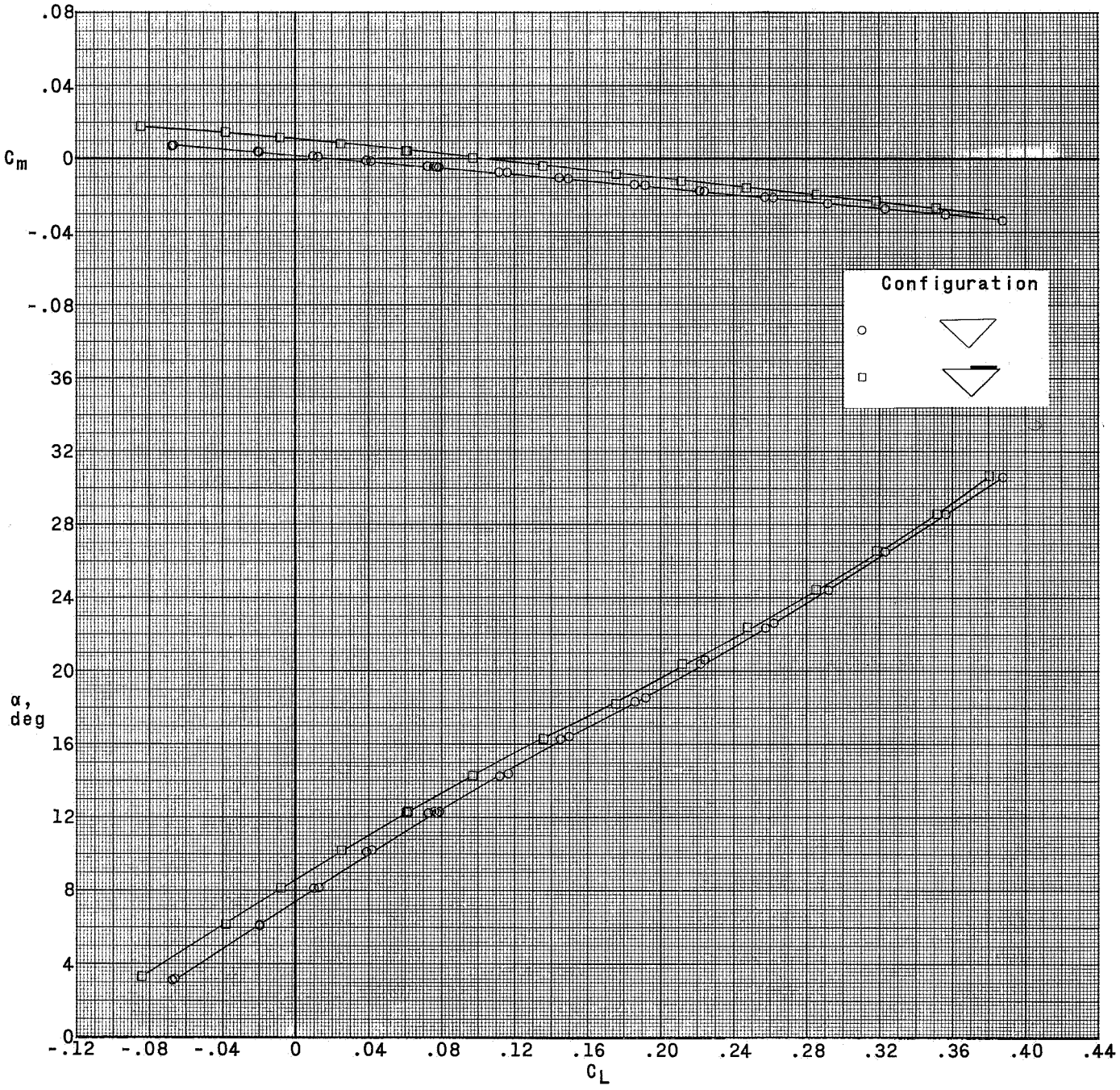

(a) M = 2.36.

Figure 9.- Effect of top-mounted flap control on aerodynamic characteristics in pitch of basic model. $\beta \approx 0^{\circ}$.

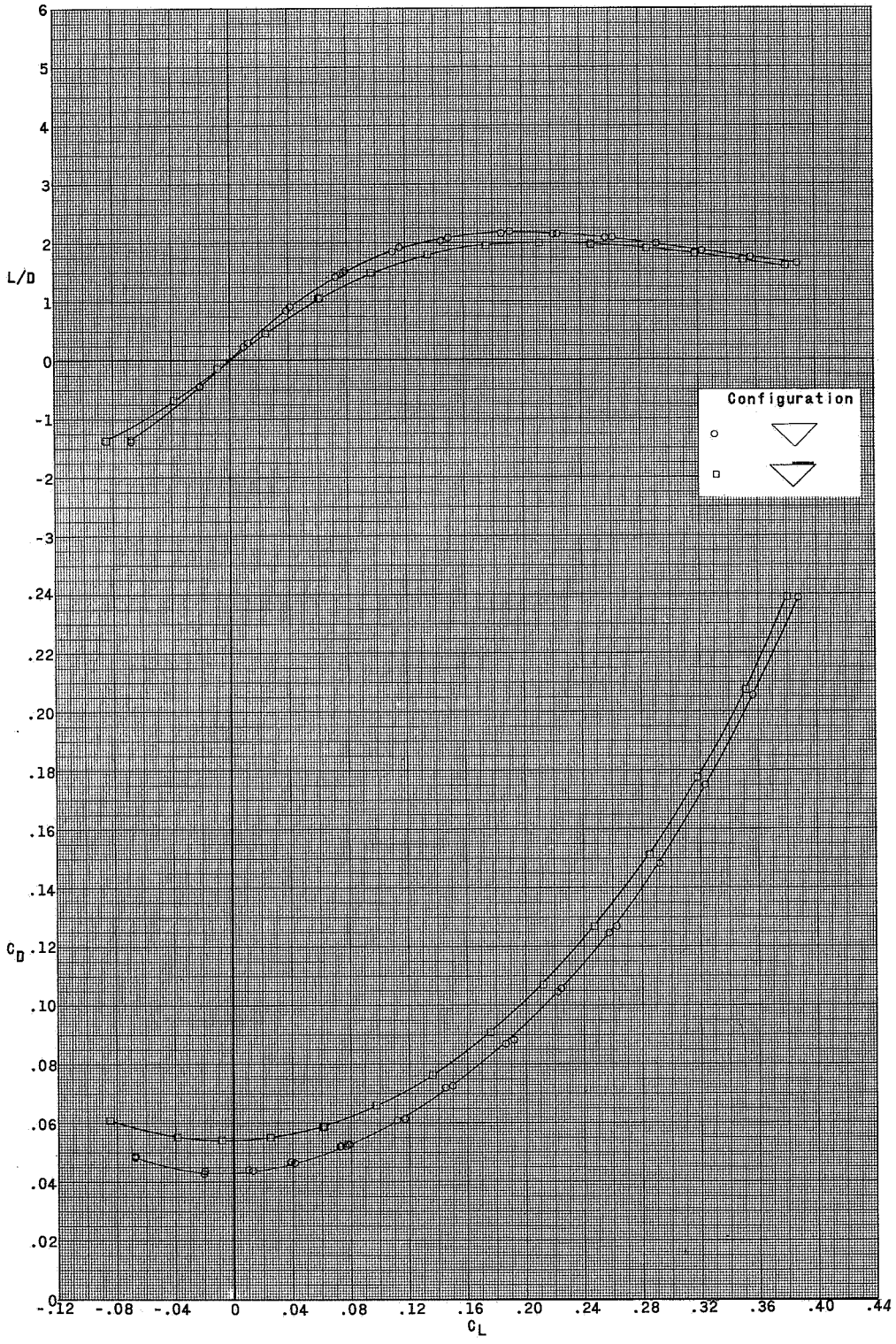

(a) Concluded.

Figure 9.- Continued.

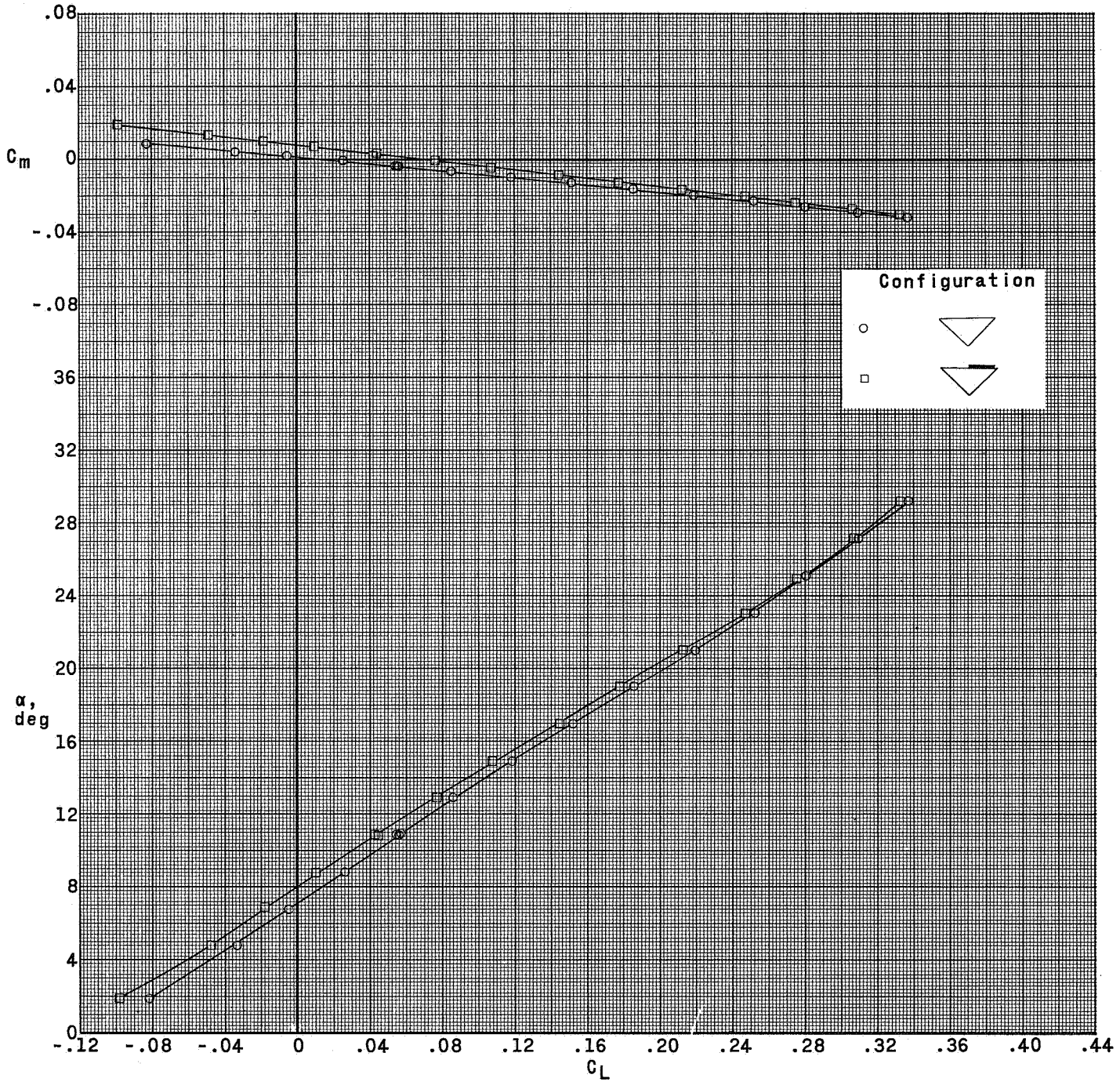

(b) M = 2.87.

Figure 9.- Continued.

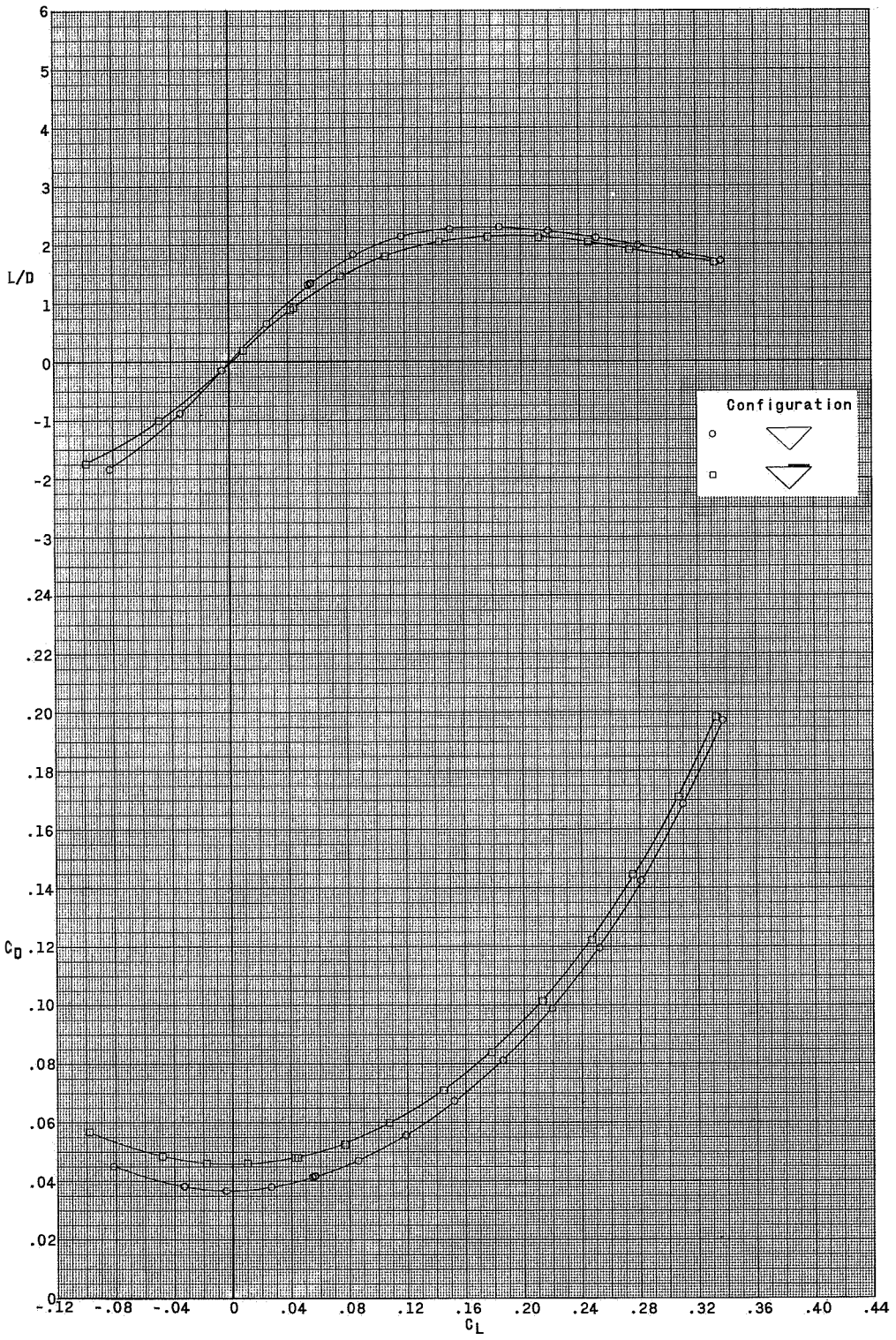

(b) Concluded.

Figure 9.- Concluded.

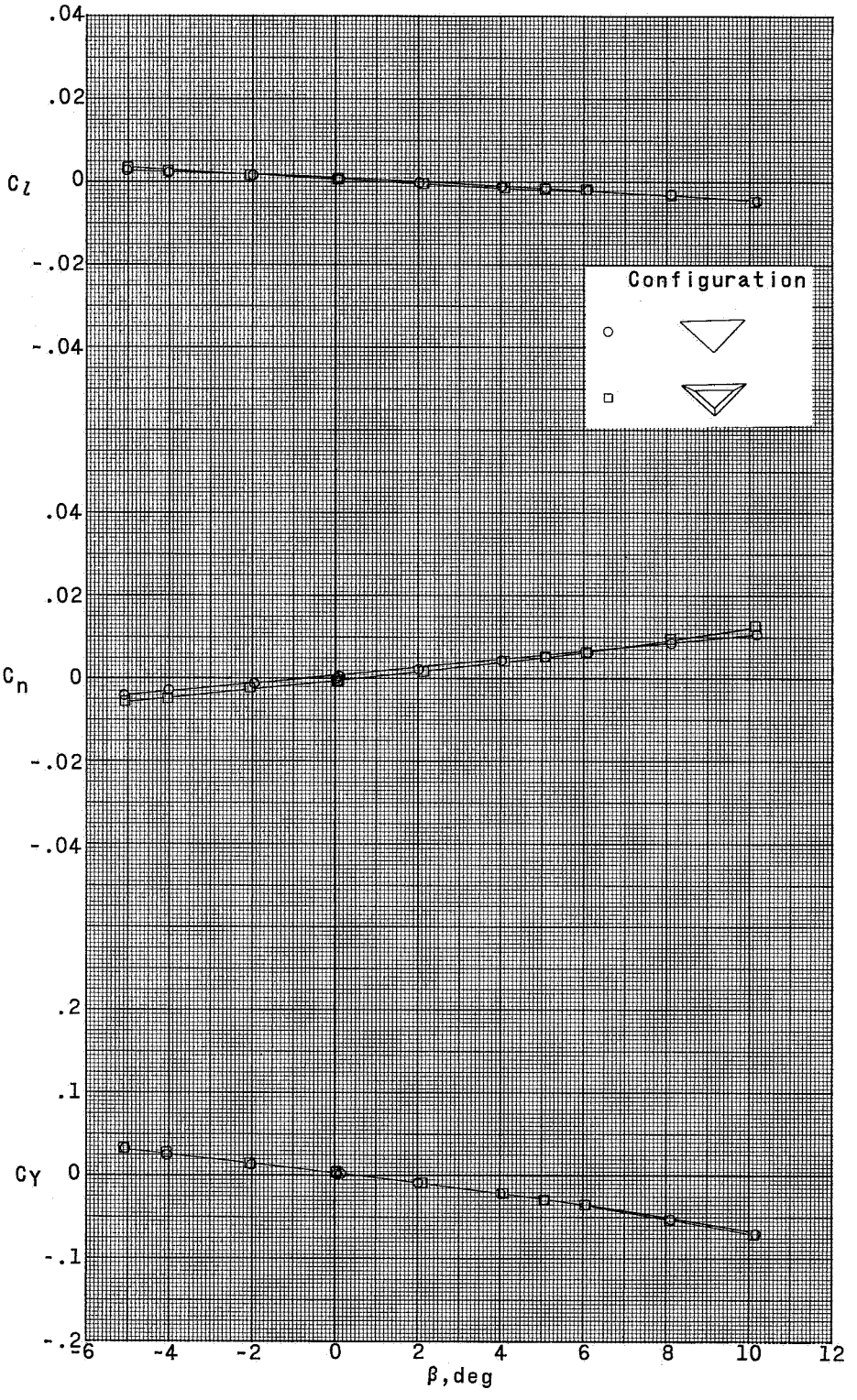

(a) M = 2.36.

Figure 10.- Aerodynamic characteristics in sideslip for the three test configurations. $\alpha \approx 2^{\circ}$.

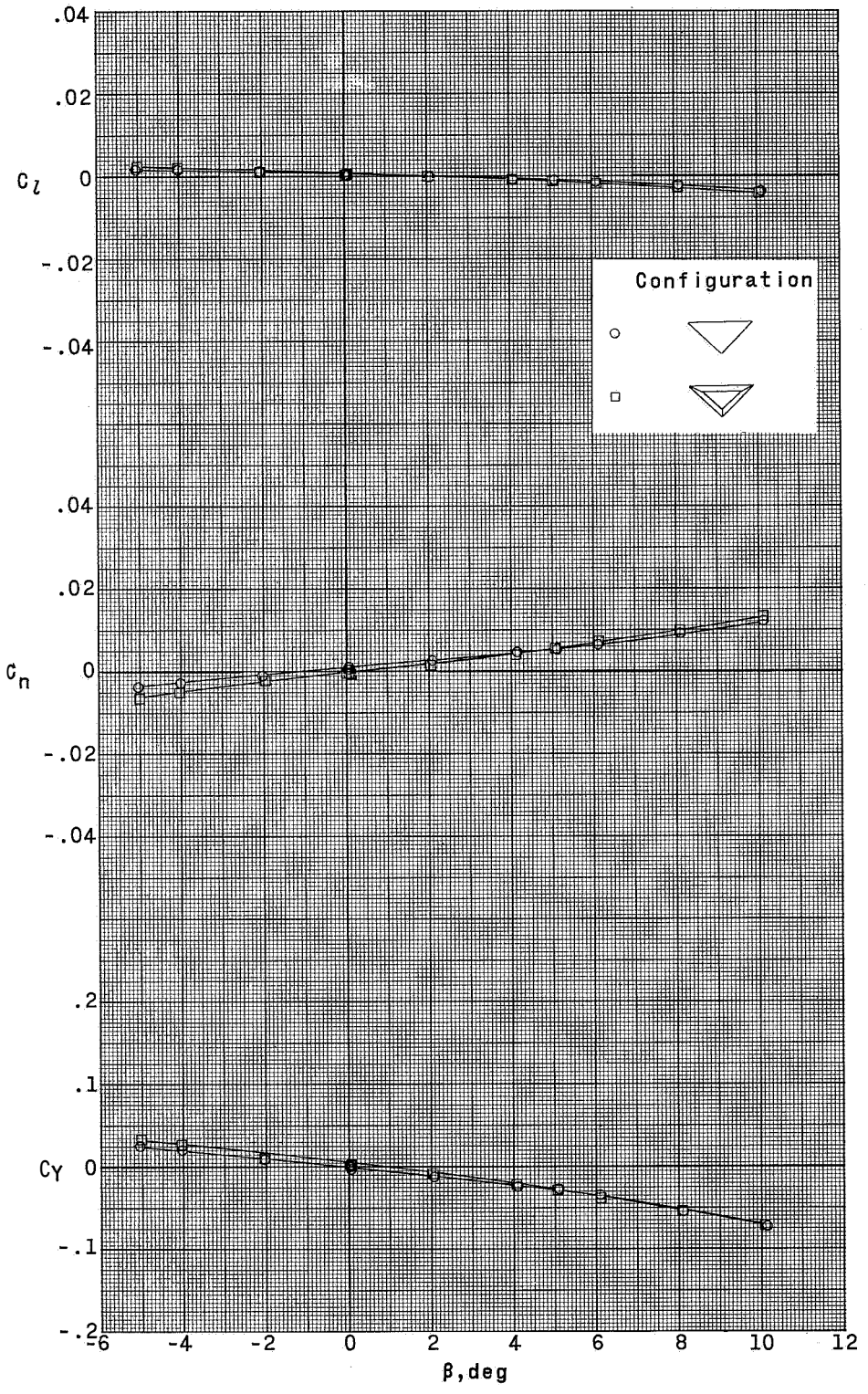

(b) M = *2.87.*

Figure 10.- **Continued.**

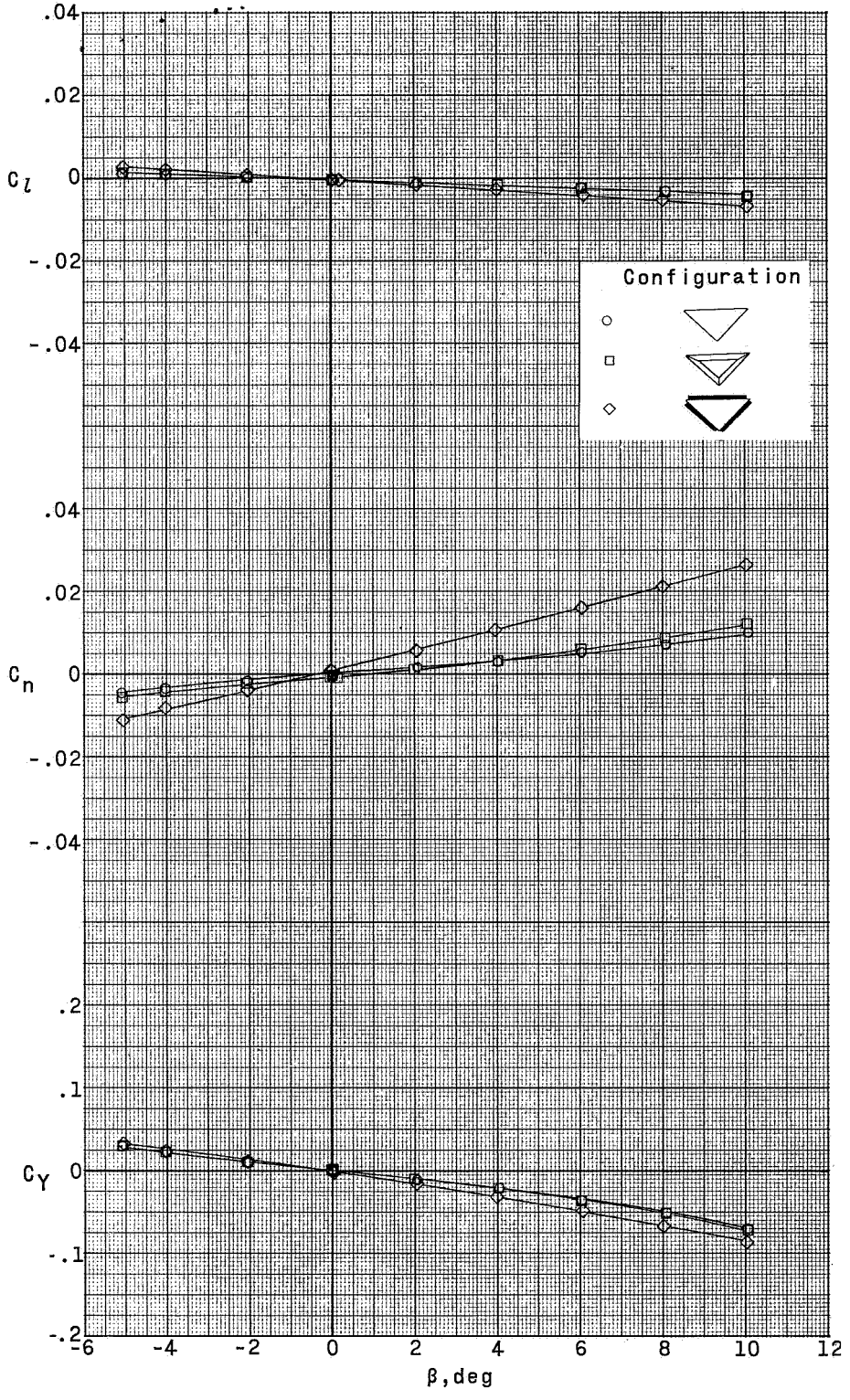

(c) M = 2.98.

Figure 10.- Continued.

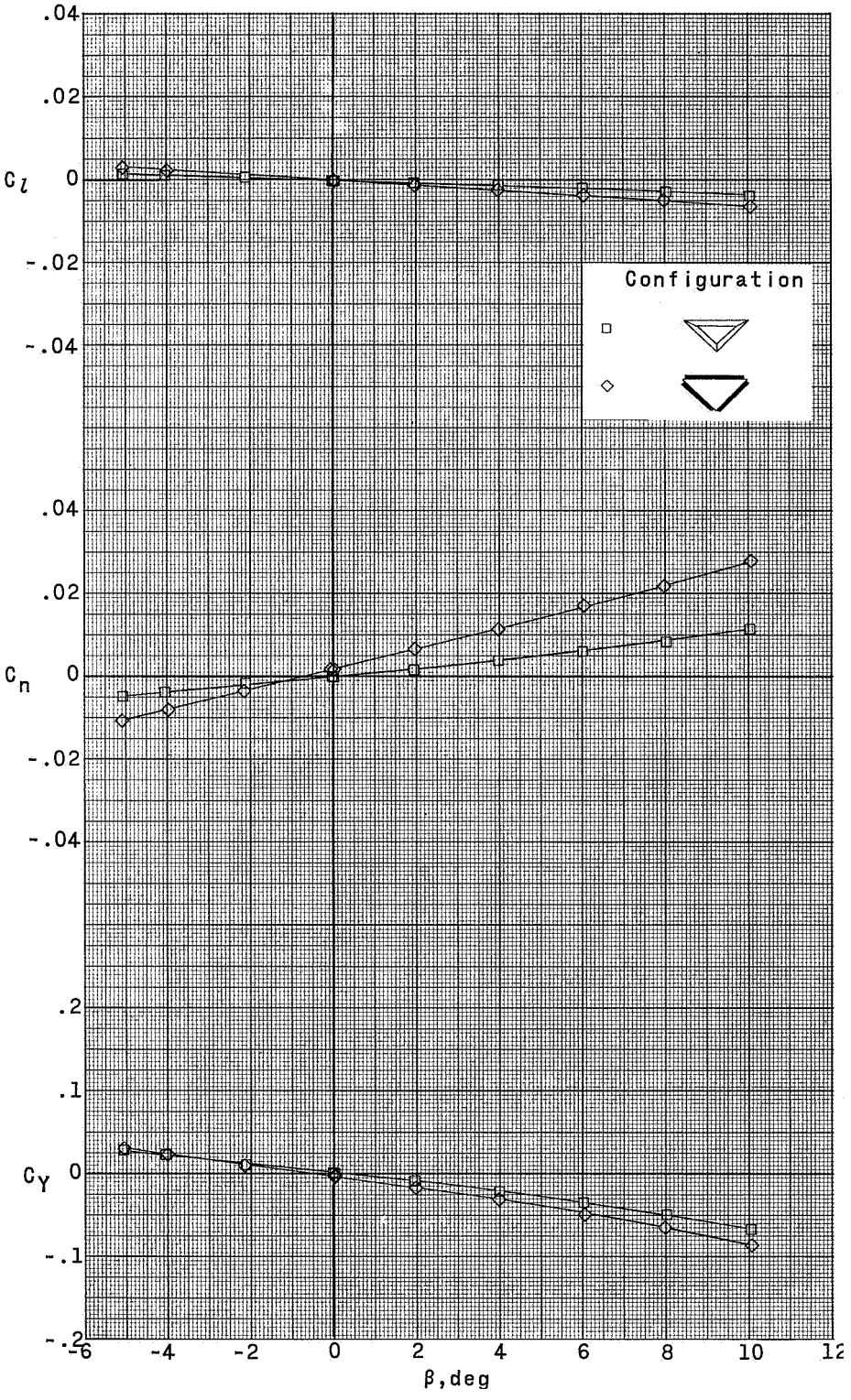

(a) M = 3.71.

Figure 10.- Continued.

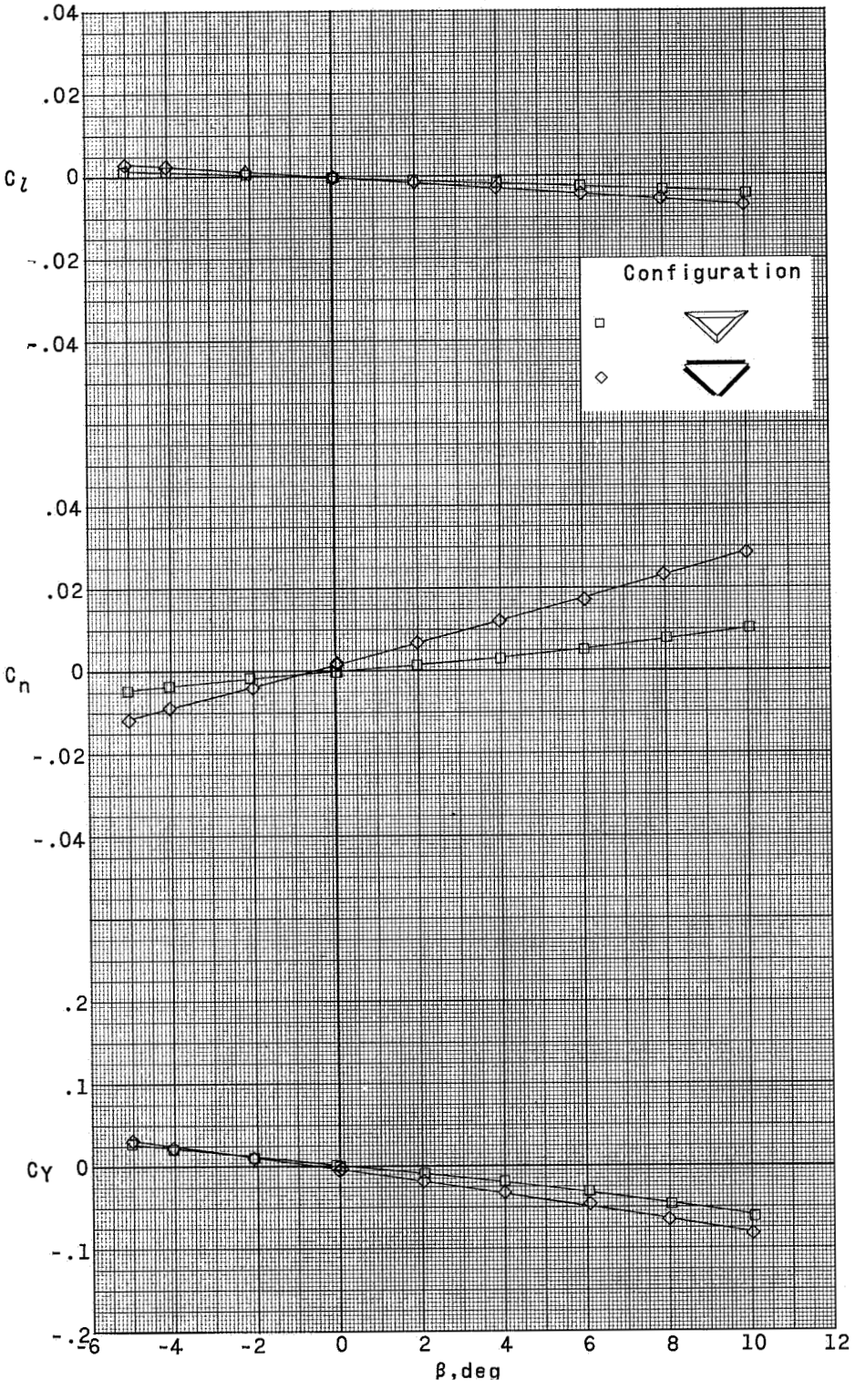

(e) M = 4.65.

Figure 10.- Concluded.

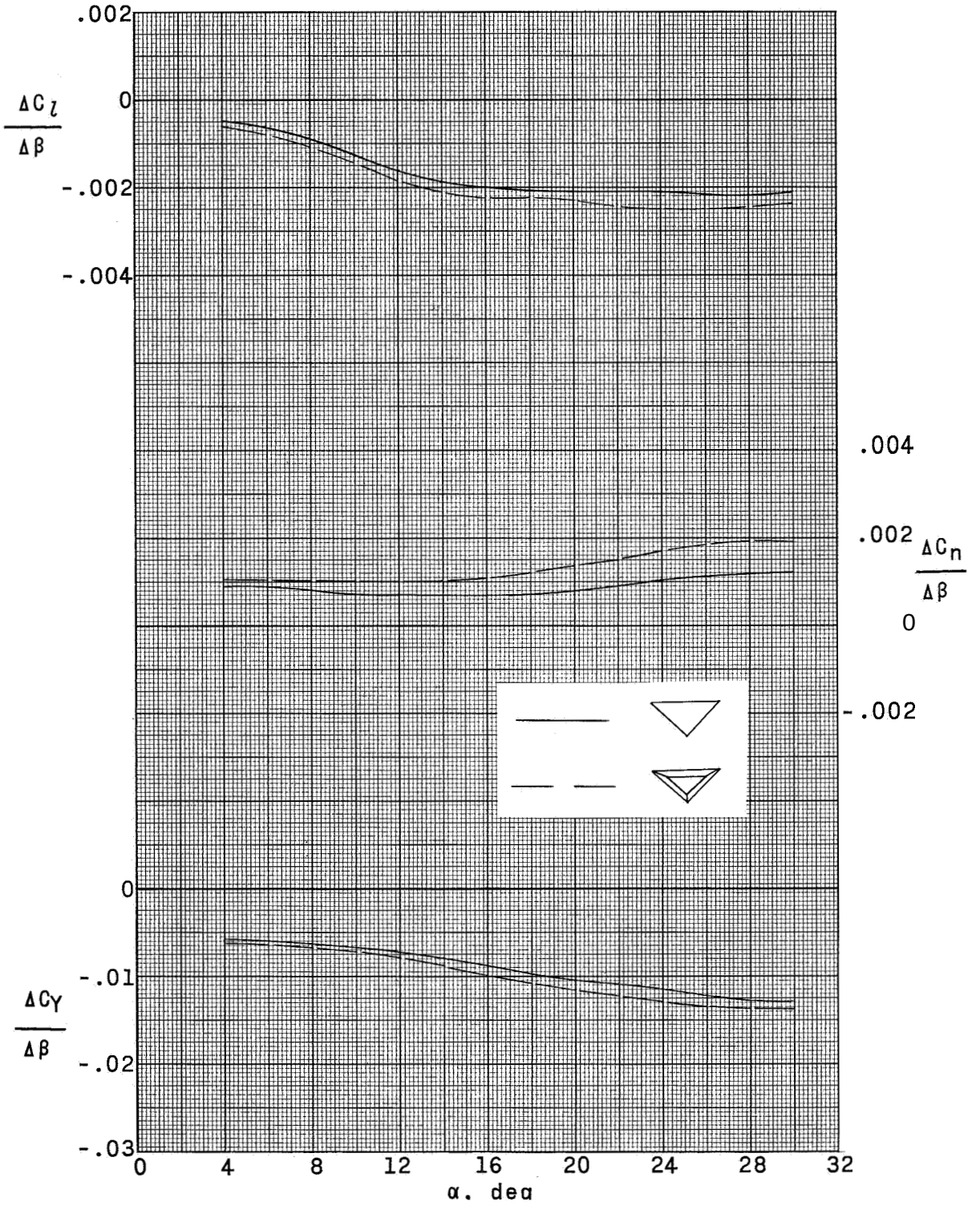

(a) M = 2.36.

Figure 11.- *Summary* of lateral parameters.

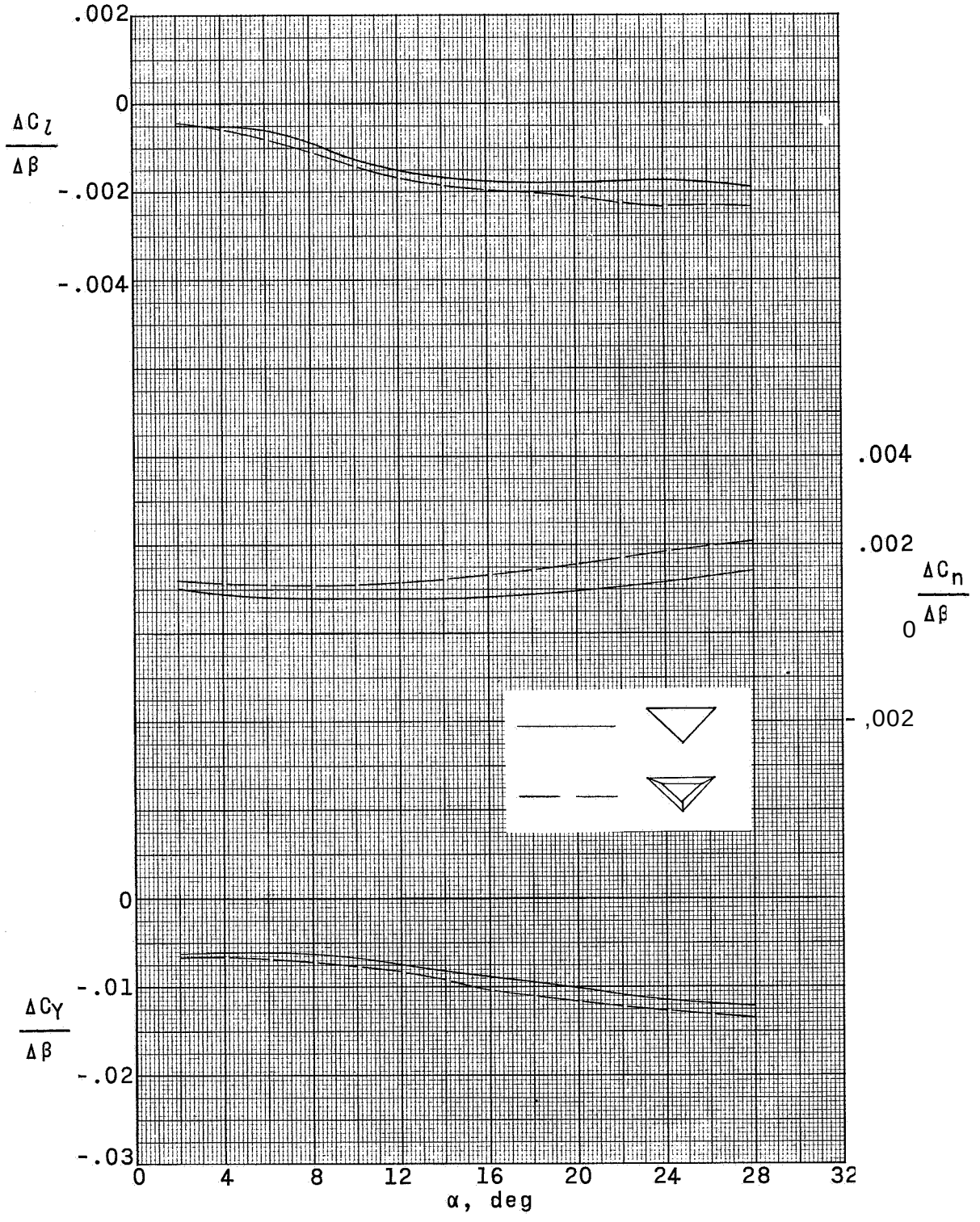

(b) M = 2.87.

Figure 11.- Continued.

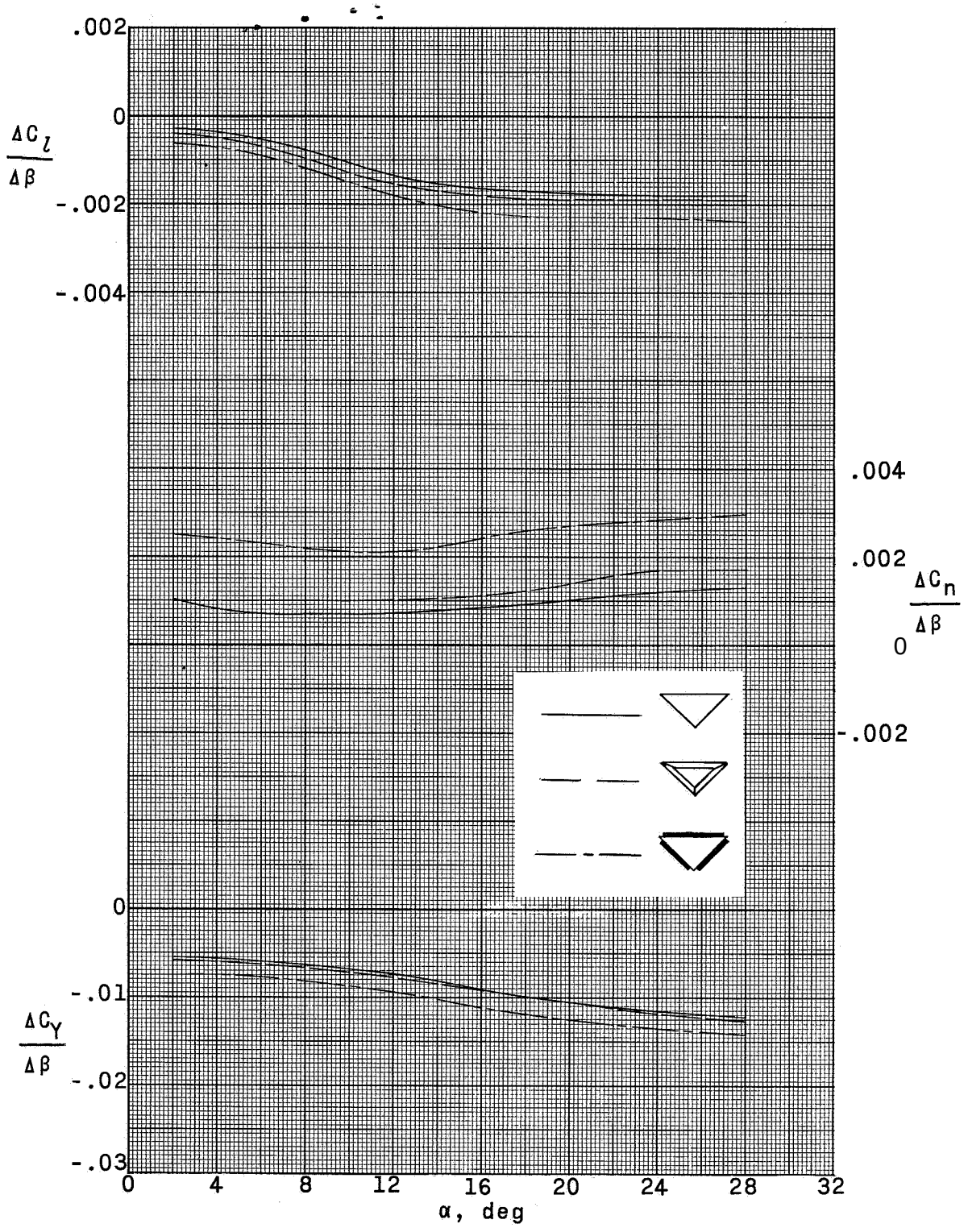

(c) M = 2.98.

Figure 11.- Continued.

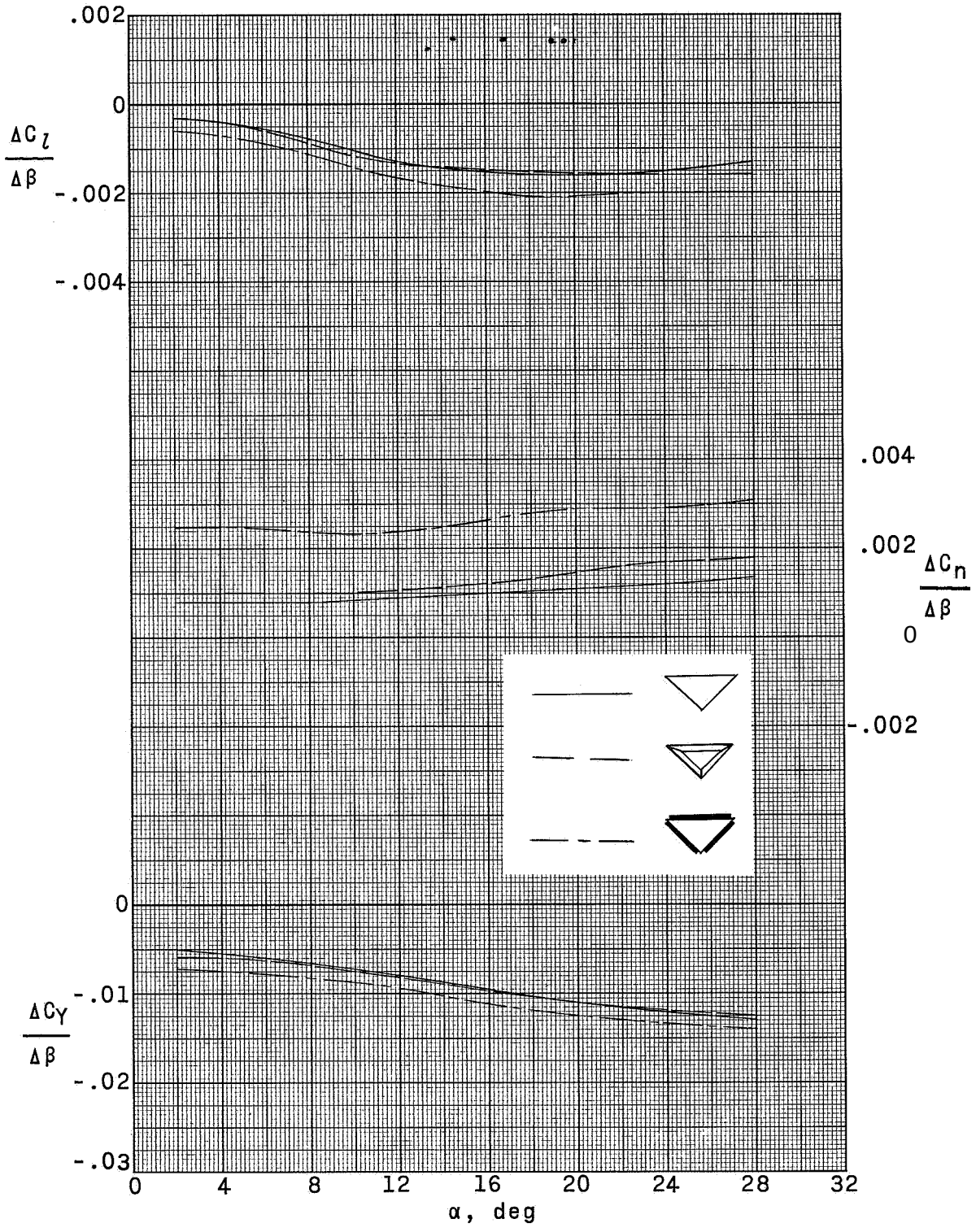

(d) M = 3.71.

Figure 11.- Continued.

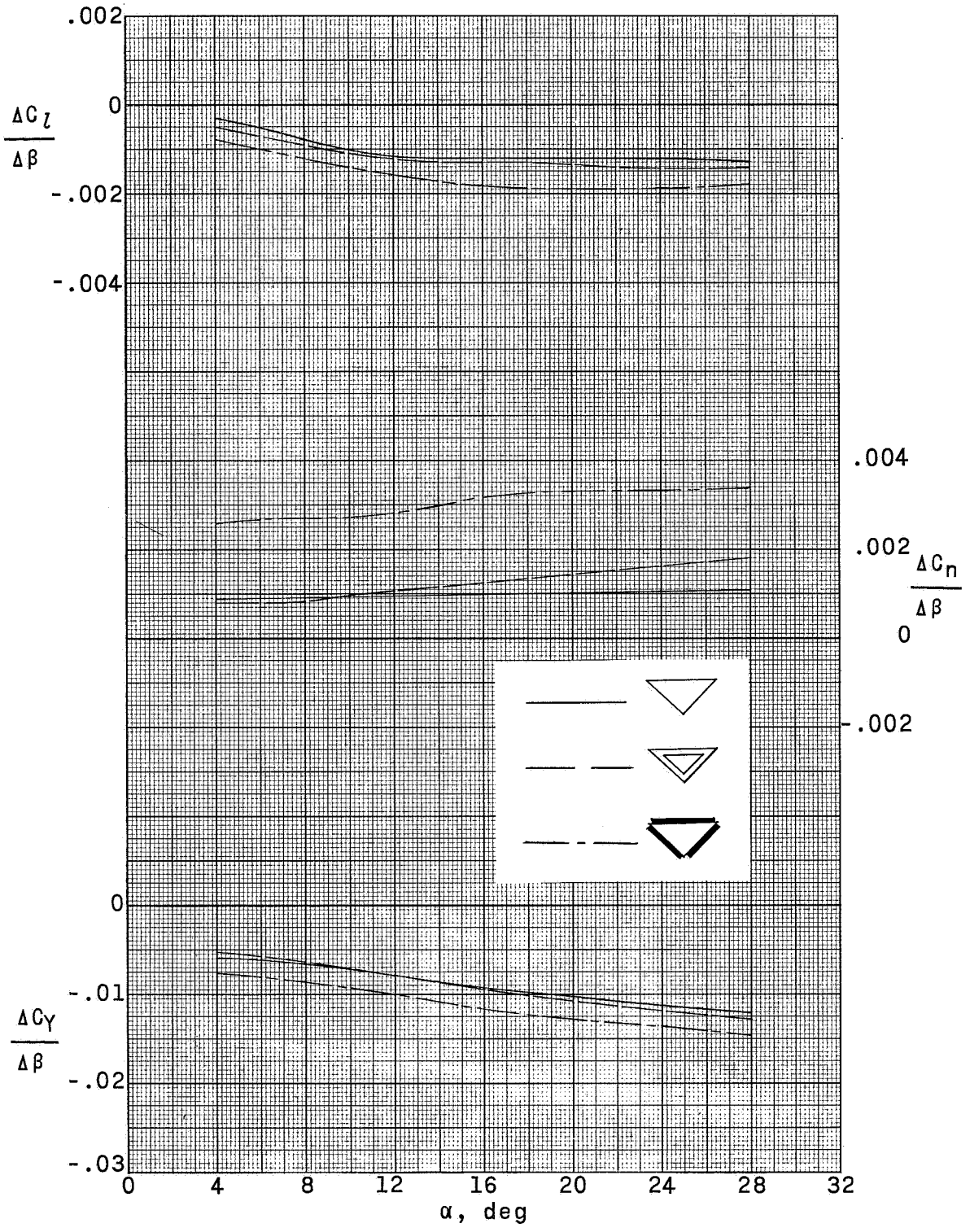

(e) M = 4.65.

Figure 11.- Concluded.

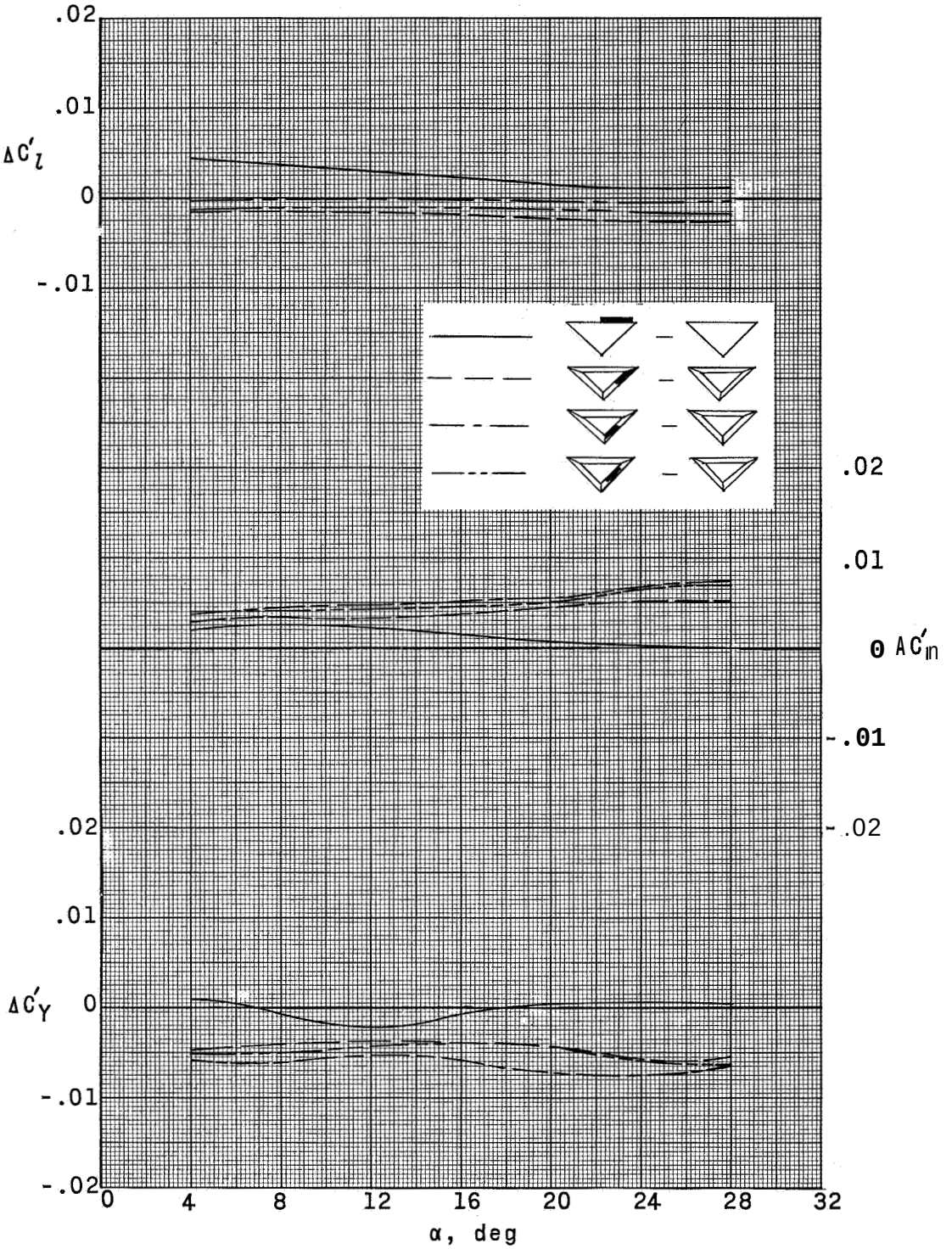

(a) M = 2.36.

Figure 12.- Effect of flap control on lateral forces and moments of basic and boattail configurations.

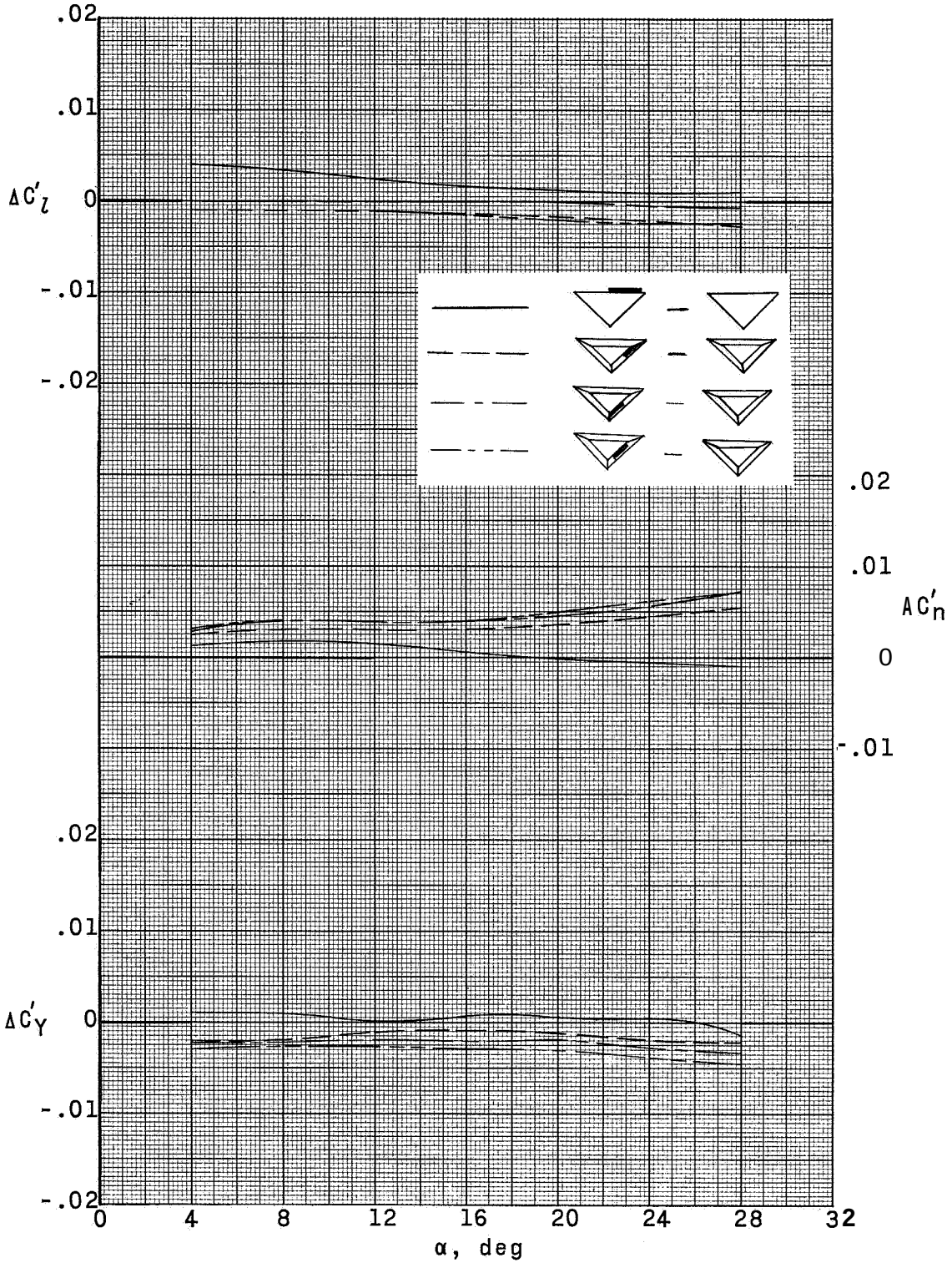

(b) M = 2.87.

Figure 12.- Continued.

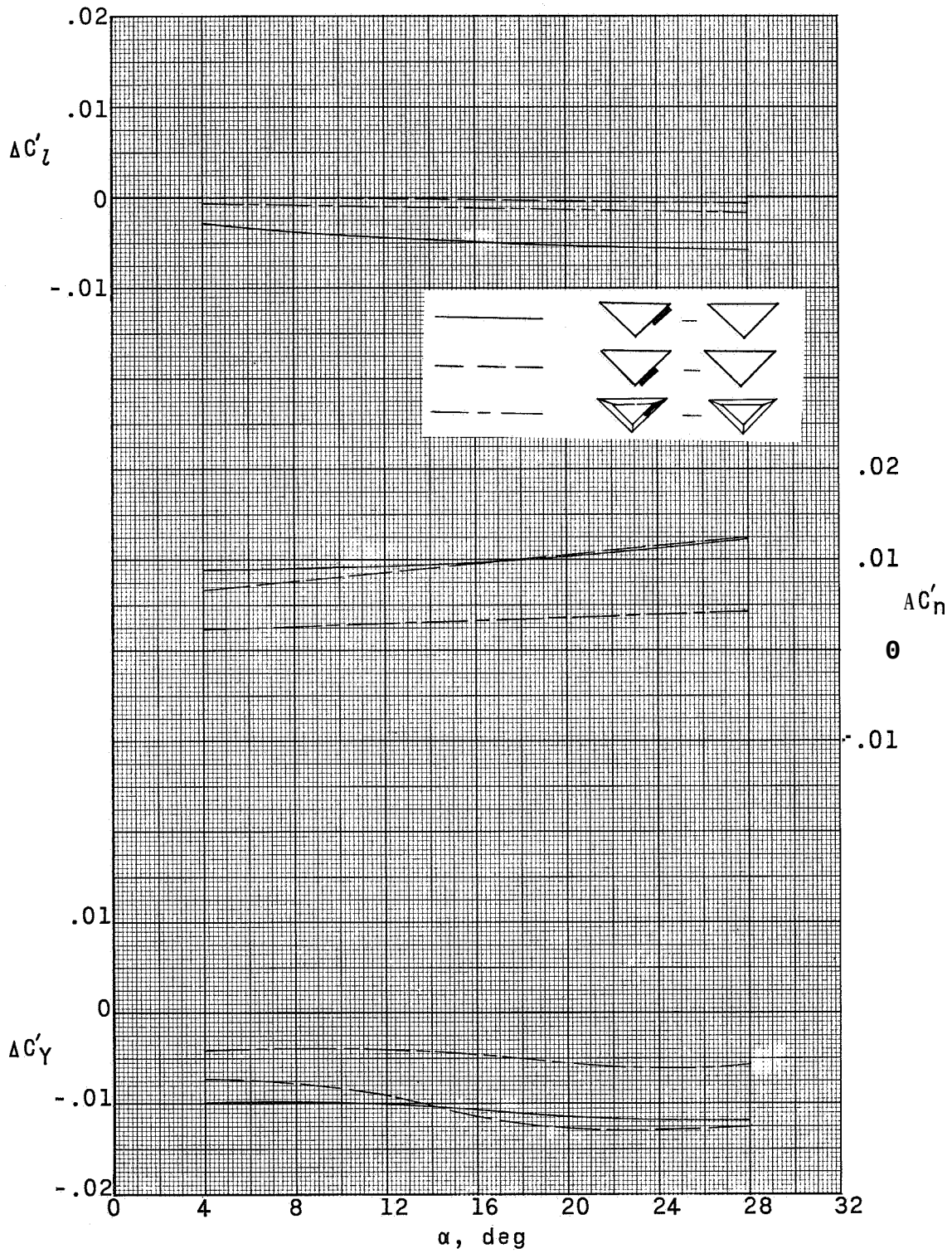

(c) M = 2.98.

Figure 12.- Continued.

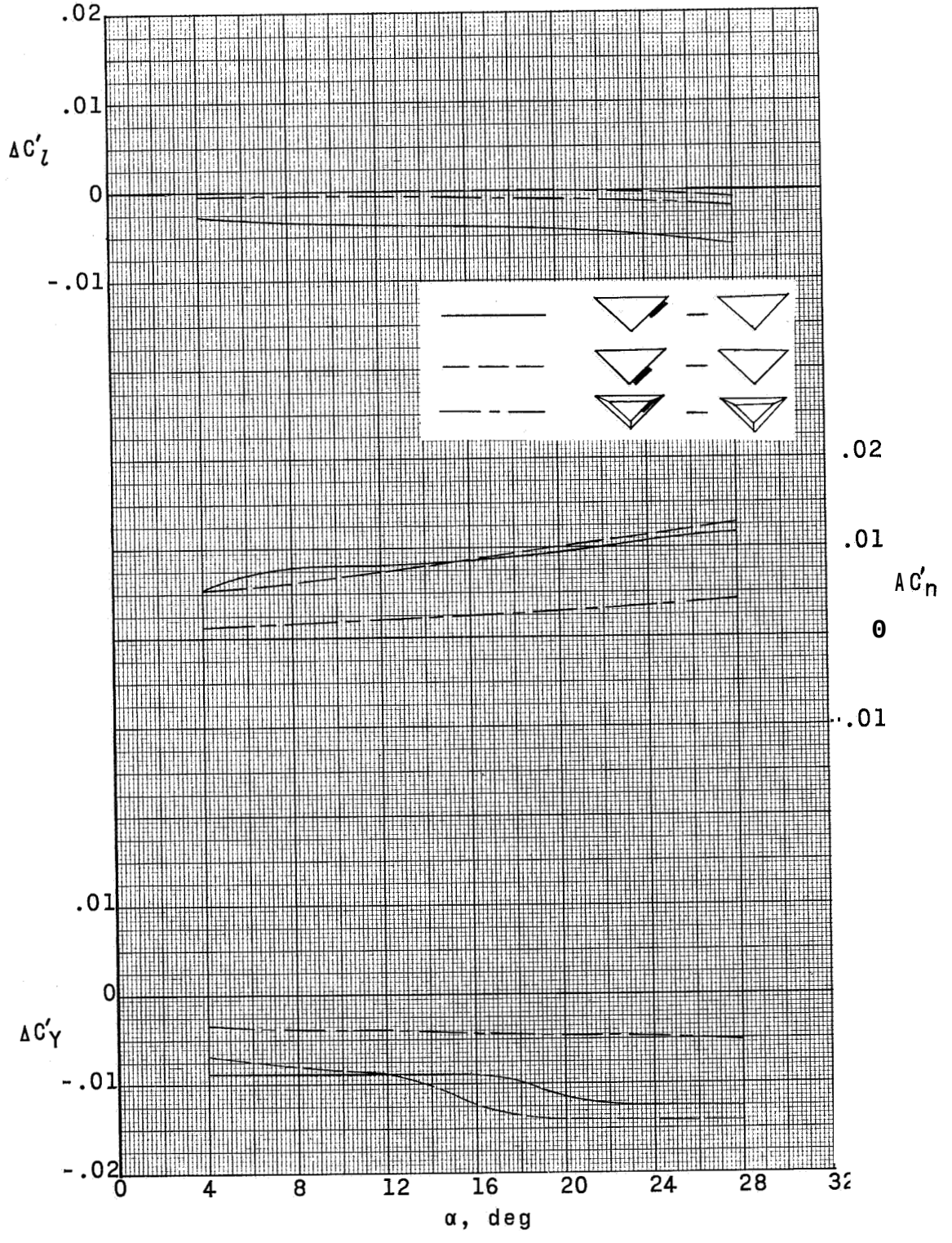

(d) M = 3.71.

Figure 12.- Continued.

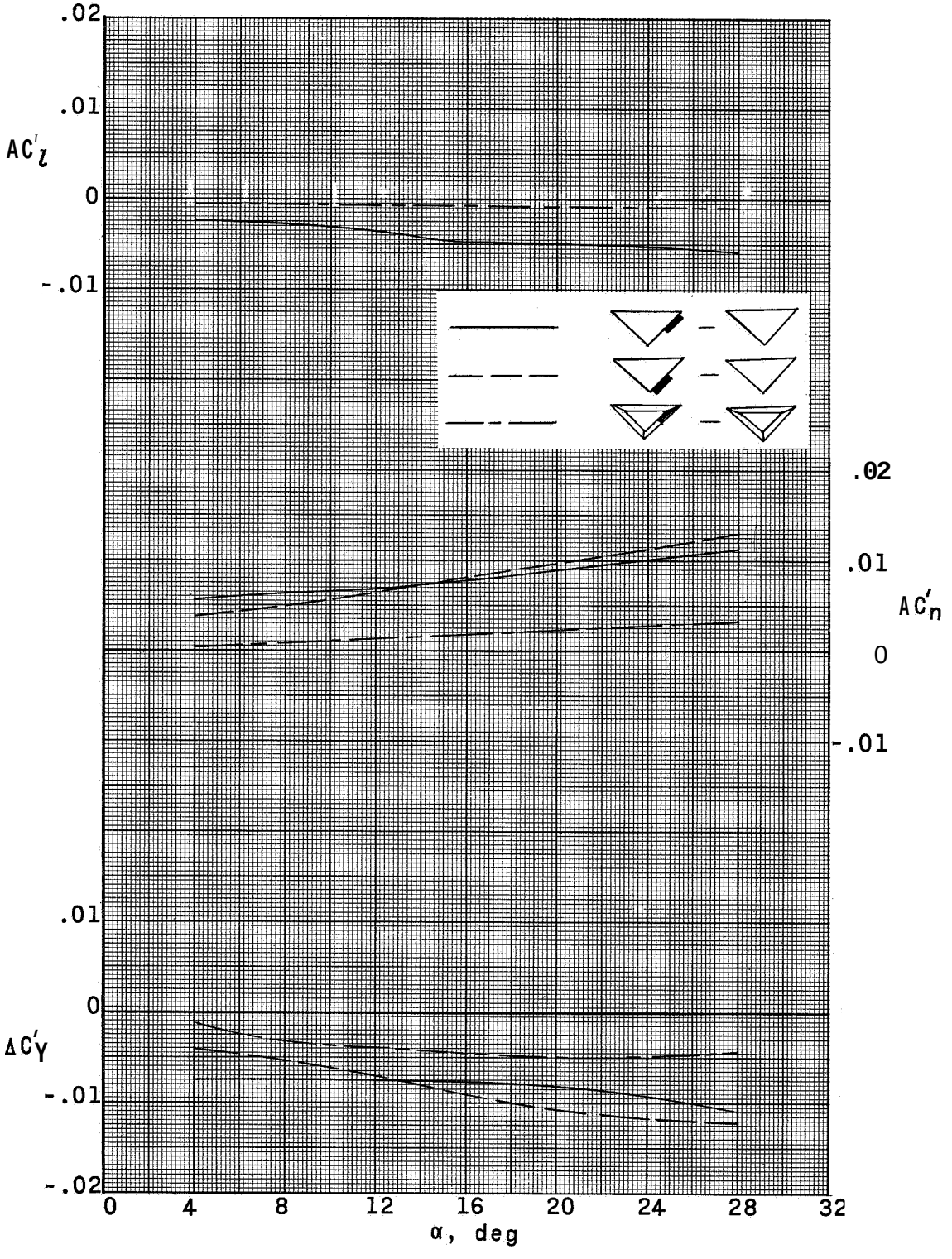

(e) M = 4.65.

Figure 12.- Concluded.